Journal of Membrane Science 430 (2013) 113–128

Contents lists available at SciVerse ScienceDirect

Journal of Membrane Science

journal homepage: www.elsevier.com/locate/memsci

Investigating the influence of diffusional coupling on mixture permeation across porous membranes

Rajamani Krishna *, Jasper M. van Baten

Van 't Hoff Institute for Molecular Sciences, University of Amsterdam, Science Park 904, 1098 XH Amsterdam, The Netherlands

ARTICLE INFO

Article history:
Received 5 November 2012
Received in revised form
5 December 2012
Accepted 6 December 2012
Available online 20 December 2012

Keywords:
Maxwell–Stefan diffusion
Correlations
Zeolites
Metal-organic frameworks
Membrane permeation
Pervaporation
Hydrogen bonding

ABSTRACT

A careful analysis of published experimental data on permeation of a variety of binary mixtures reveals that there are fundamentally two types of diffusional coupling effects that need to be recognized. The first type of coupling occurs when the less-mobile species slows down its more mobile partner by not vacating an adsorption site quick enough for its more mobile partner to occupy that position. Such slowing-down effects, also termed correlation effects, are quantified by the exchange coefficient $Đ_{12}$ in the Maxwell–Stefan (M–S) formulation. The parameter $Đ_1/Đ_{12}$, quantifying the degree of correlations, is strongly dependent on the pore size, topology and connectivity and reasonable estimates are provided by molecular dynamics (MD) simulations. In cage-type structures (e.g. CHA, DDR, LTA, and ZIF-8) in which adjacent cages are separated by narrow windows correlations are weak, and $Đ_1/Đ_{12} \approx 0$ is a good approximation. On the other hand correlations are particularly strong in structures consisting of one-dimensional channels (e.g. NiMOF-74), or intersecting channels (e.g. MFI) structures; in these cases the values of $Đ_1/Đ_{12}$ are in the range 1–5. A wide variety of experimental data on binary mixture permeation can be quantitatively modeled with the Maxwell–Stefan equations using data inputs based on unary permeation experiments, along with $Đ_1/Đ_{12}$ values suggested by MD. The second type of coupling occurs as a consequence of molecular clustering due to hydrogen bonding. Such clustering effects, commonly prevalent in alcohol/water pervaporation, can cause mutual slowing-down of partner molecules in the mixture. When molecular clustering occurs the Maxwell–Stefan diffusivity of a species in the mixture, $Đ_i$, cannot be identified with that obtained from unary permeation.

1. Introduction

The proper description of permeation of mixtures across porous membranes consisting of thin layers of ordered crystalline materials such as zeolites (crystalline aluminosilicates), metal-organic frameworks (MOFs), and zeolitic imidazolate frameworks (ZIFs) is important in development and design of a variety of industrially important separation processes, such as CO_2 capture, natural gas purification, fuel gas purification and pervaporation [1–8]. For separation of a binary mixture, the permeation selectivity, S_{perm}, is commonly defined as the ratio of the component permeances across the porous layer

$$S_{perm} = \frac{\Pi_1}{\Pi_2} = \frac{N_1/\Delta p_1}{N_2/\Delta p_2} \tag{1}$$

where the fluxes N_i, are defined in terms of the cross-sectional area of the membrane (see schematic in Fig. 1). The Maxwell–Stefan (M–S) formulation for mixture diffusion is most commonly used for modeling membrane permeation [5,9–14]. Solution of the M–S equations for steady-state binary mixture permeation results in the following set of equations for the permeation fluxes

$$N_1 = \frac{\rho Đ_1}{\delta}\left[\frac{(1+x_1 Đ_2/Đ_{12})\Delta q_1 + x_1 Đ_2/Đ_{12}\Delta q_2}{1+x_1 Đ_2/Đ_{12}+x_2 Đ_1/Đ_{12}}\right] \tag{2}$$

and

$$N_2 = \frac{\rho Đ_2}{\delta}\left[\frac{x_2 Đ_1/Đ_{12}\Delta q_1 + (1+x_2 Đ_1/Đ_{12})\Delta q_2}{1+x_1 Đ_2/Đ_{12}+x_2 Đ_1/Đ_{12}}\right] \tag{3}$$

In the derivations of the Eqs. (2) and (3), details of which are provided in the Supplementary Material accompanying this publication, the resistance of the support layer is ignored. Furthermore, the micro-porous crystalline layer is considered to be defect-free, and inter-grain boundary resistances have not been accounted for.

The molar loadings, q_i, in the adsorbed phase at either face of the membrane are obtained from adsorption equilibrium. In all the calculations presented is this study, the adsorption equilibrium is determined using the Ideal Adsorbed Solution Theory of

* Corresponding author. Tel.: +31 20 6270990; fax: +31 20 5255604.
E-mail address: r.krishna@uva.nl (R. Krishna).

0376-7388/$ - see front matter © 2012 Elsevier B.V. All rights reserved.
http://dx.doi.org/10.1016/j.memsci.2012.12.004

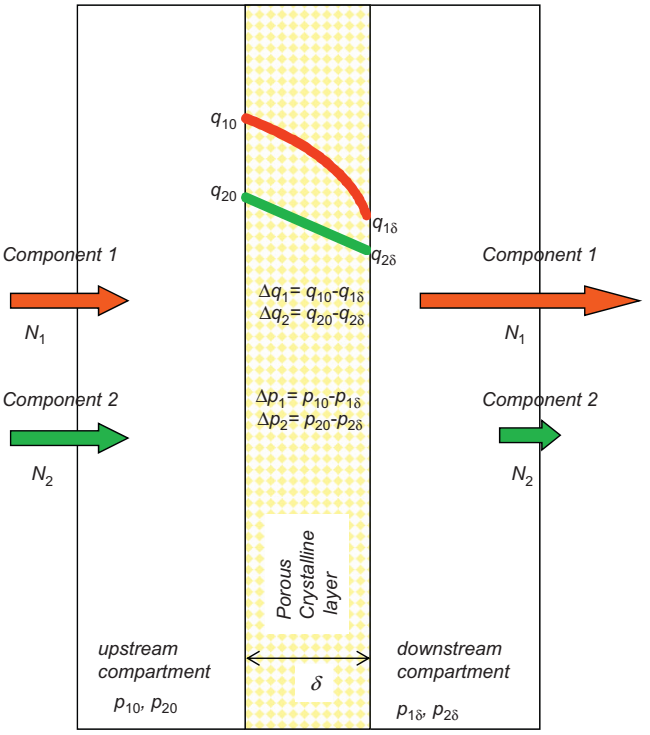

Fig. 1. Schematic of binary mixture permeation across a porous crystalline layer.

Myers and Prausnitz [15], on the basis of pure component isotherm fits. The x_i are the component mole fractions in the adsorbed phase within the membrane

$$x_1 = q_1/(q_1+q_2); \quad x_2 = q_2/(q_1+q_2) \tag{4}$$

The calculation of x_i using the upstream loadings is sufficiently accurate for the estimation of the permeation fluxes.

There are basically two different types of M–S diffusivities. The $Đ_1$ and $Đ_2$ characterize the interactions, in the broadest sense, with the pore walls. The $Đ_{12}$ is the exchange coefficient which quantify diffusional coupling between the two components. At the molecular level, the $Đ_{12}$ reflect how the facility for transport of species 1 correlates with that of species 2. In subsequent discussions, it is convenient to define the ratio $(Đ_1/Đ_{12})$ as a reflection of the degree of correlations. The diffusional characteristics of the porous crystalline layer is therefore described by three separate independent parameters: (a) the two membrane transport coefficients $\rho Đ_1/\delta$, and $\rho Đ_2/\delta$, and (b) the degree of correlations $Đ_1/Đ_{12}$.

In assessing the separation capability of any membrane for a given separation task it is useful to also define the adsorption selectivity, S_{ads}, in terms of the component loadings and partial pressures in the upstream compartment.

$$S_{ads} = \frac{q_{10}/q_{20}}{p_{10}/p_{20}} \tag{5}$$

A further useful metric is the diffusion selectivity of the membrane, S_{diff}

$$S_{diff} = \frac{S_{perm}}{S_{ads}} = \frac{Đ_1}{Đ_2}\frac{(1+Đ_2/Đ_{12})}{(1+Đ_1/Đ_{12})} \tag{6}$$

where the second right member in Eq. (6) is derived for the commonly valid assumption that the downstream partial pressures, and component loadings are negligible in comparison with the corresponding upstream values (detailed derivations are provided in the Supplementary Material). For the special limiting case for which the degree of correlations is negligible small, Eq. (6) simplifies to yield

$$S_{diff} = \frac{Đ_1}{Đ_2}; \quad \text{negligible correlations} \tag{7}$$

A special distinguishing feature of membrane separations, in contrast to other competitive technologies such as pressure swing adsorption (PSA) devices, is that the permeation selectivity S_{perm} is governed not only by S_{ads} but also by the diffusional characteristics. PSA units are largely, though not exclusively, governed by S_{ads} but membrane-based separations offer the possibility of also exploiting S_{diff} to significantly enhance the obtained value of S_{perm}.

There are three major objectives of the investigations reported here.

The first objective is to identify conditions and systems for which the diffusional coupling effects can be assumed to be of negligible significance. This scenario corresponds to the limiting case in which $(Đ_1/Đ_{12}) \to 0$ and, as a consequence, Eqs. (2) and (3) simplify to yield

$$N_1 = \frac{\rho Đ_1}{\delta}\Delta q_1; \quad N_2 = \frac{\rho Đ_2}{\delta}\Delta q_2; \quad \text{negligible correlations} \tag{8}$$

The second objective is to identify and examine systems for which the correlation effects are significant. In such cases we seek to establish the applicability of M–S Eqs. (2) and (3) in describing mixture permeation characteristics by estimating the membrane transport coefficients $\rho Đ_1/\delta$, and $\rho Đ_2/\delta$ from unary permeation data. We aim to show that a clever choice of the membrane material, with the appropriate degree of correlations, will serve to significantly enhance the permeation selectivity.

The third objective is to identify systems for which the $\rho Đ_1/\delta$, and $\rho Đ_2/\delta$ characterizing mixture permeation cannot be identified with those obtained from unary permeation.

2. Comparing the degree of correlations in different host materials

There is no experimental technique for direct determination of the exchange coefficients $Đ_{12}$, that quantify molecule–molecule interactions. For this reason we use molecular dynamics (MD) simulation data from the literature [13,14,16–19] to obtain the necessary insights and inputs. For convenience, a summary of available MD simulation data, and the interpretation thereof, is provided as Supplementary Material.

For mesoporous materials, such as BTP-COF, the values of the exchange coefficient $Đ_{12}$ are the nearly the same as the binary fluid phase M–S diffusivity, $Đ_{12,\,fl}$, over the entire range of pore concentrations. A similar result holds for mesopores in the 20–100 Å size range [20]. Procedures for estimation of the $Đ_{12,\,fl}$ are available in Poling et al. [21], and therefore this provides a convenient starting point for the estimation of the $Đ_{12}$.

For micro-porous materials, the exchange coefficient $Đ_{12}$ cannot be directly identified with the corresponding fluid phase diffusivity $Đ_{12,\,fl}$ because the molecule–molecule interactions are also significantly influenced by molecule–wall interactions. This is underscored by MD data for $Đ_{12}$ for six binary mixtures, with $q_1 = q_2$, in a variety of micro-porous hosts; see Fig. 2. For every guest/host combination, at any total mixture pore concentration, $c_t = (q_1+q_2)/V_p$, the $Đ_{12}$ is lower than the value of $Đ_{12,\,fl}$. The extent of lowering can be quantified by defining the fraction F

$$F \equiv Đ_{12}/Đ_{12,\,fl} \tag{9}$$

Every guest/host combination can be characterized by a constant fraction F, that are determined by data fitting; the complete data sets are available in the Supplementary Material

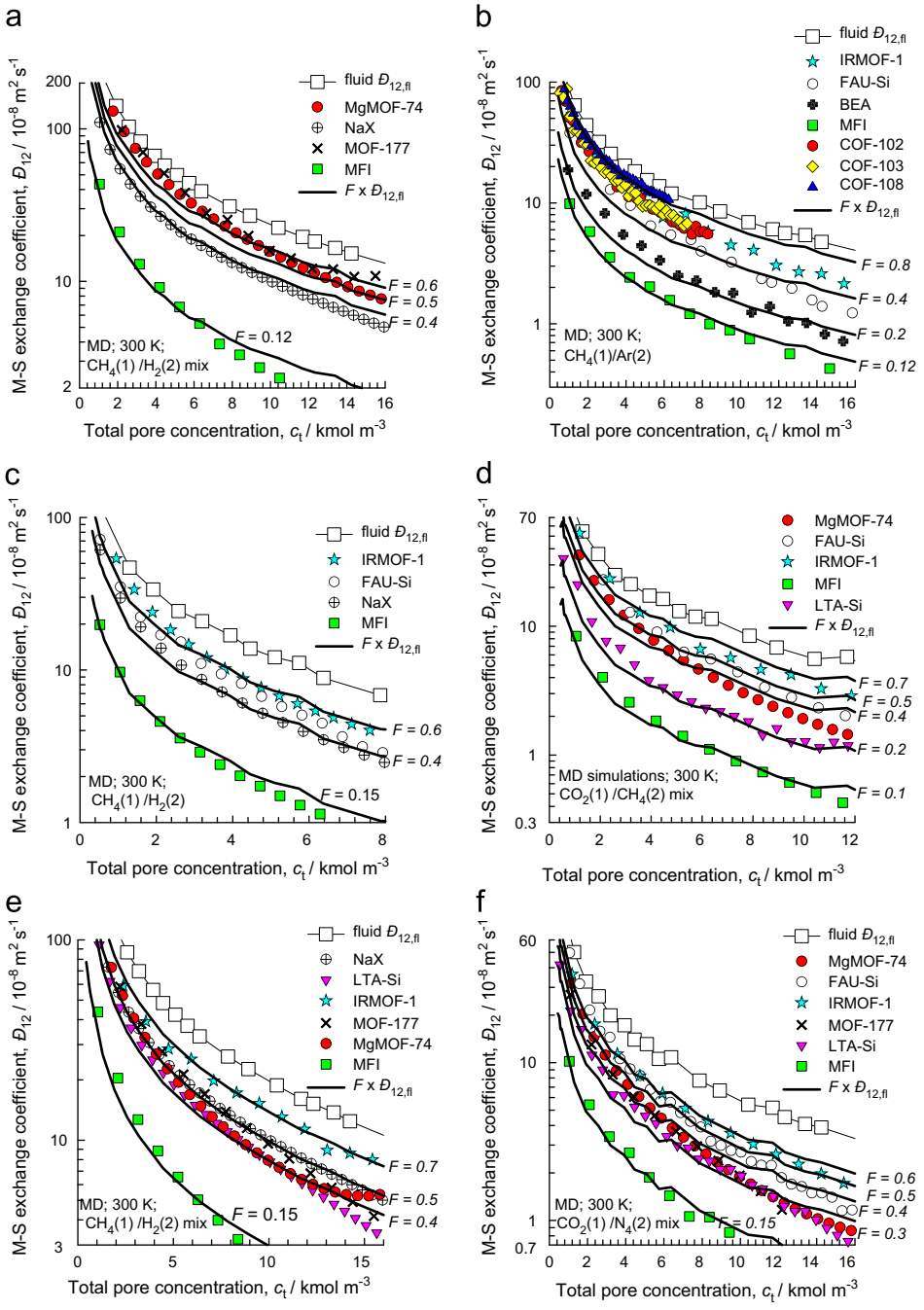

Fig. 2. The M–S binary exchange coefficients $Đ_{12}$, for diffusion of equimolar ($c_1 = c_2$) binary mixtures (a) H_2/CH_4, (b) CH_4/Ar, (c) CH_4/C_2H_6, (d) CH_4/CO_2, (e) H_2/CO_2, and (f) CO_2/N_2 at 300 K in a variety of host materials as a function of the total pore concentration, c_t. The $Đ_{12,\,fl}$ for binary fluid phase mixture diffusion, obtained from independent MD simulations, is also presented in square symbols, along with continuous solid lines that represent the fraction F times $Đ_{12,\,fl}$ The MD data are culled from our previous publications [14,16–20,22,87–91]. A more complete set of data is available in the Supplementary material.

accompanying this publication. For "open" structures, with large pore volumes, V_p, the values of F are closer to unity. For example, for CH_4/Ar diffusion in IRMOF-1, COF-102, COF-103, and COF-108, the values are F=0.6, 0.65, 0.65, and 0.8, respectively, increasing with increasing pore void fractions, ϕ. Remarkably, for IRMOF-1, the factor F is in the narrow range of 0.6–0.7 for every guest mixture investigated.

At the other end of the spectrum, materials with low pore volumes, the values of the fraction F lie significantly below unity. In MFI that has a set of intersecting channels, F lies in the range of 0.1–0.15 for all mixtures. For BEA, also with intersecting channels, but with a slightly higher pore void fraction, we obtain F=0.2. For materials such as FAU, NaX, NaY, LTA, and MgMOF-74 with intermediate void fractions, the values of F fall in the range 0.3–0.6.

In summary, for micro-porous materials, the $Đ_{12}$ are lower than the corresponding fluid phase diffusivity $Đ_{12,\,fl}$ by a factor, F, that depends on the pore volume, pore size, and connectivity of the host materials. The stronger the degree of confinement, the smaller is the value of F [13,20]. Within the 5.5 Å intersecting channels of MFI zeolite, the $Đ_{12}$ is about a tenth of the value for the corresponding fluid mixture, when compared at the same

total molar concentration $c_t=(q_1+q_2)/V_p$ within the pores, i.e. $F\approx 0.1$. Within the 1D, 11 Å sized hexagonal-shaped channels of MgMOF-74, and NiMOF-74, the value of F is in the range of 0.4–0.6. For FAU-Si, NaY, and NaX that has 7.4 Å sized windows separating 11 Å sized cages, the values of F are in the range 0.3–0.6. For IRMOF-1, the value of F is in the range of 0.6–0.7.

For the purposes of interpreting experimental data on membrane permeation we need information on the degrees of correlation, $Đ_1/Đ_{12}$. Fig. 3 shows MD data on $Đ_1/Đ_{12}$ for diffusion of six different mixtures in a variety of host materials, expressed as a function of the total concentration, c_t, of the adsorbed mixture within the pores. The use of pore concentrations c_t rather than the molar loadings affords a fairer comparison of different host materials as explained in previous works [20]. For any guest/host combination, $Đ_1/Đ_{12}$ is seen to increase as the pore concentration increases; this implies that correlation effects are expected to be stronger for membrane separations operating at higher pressures. The degree of correlations is weakest in cage-type structures such as

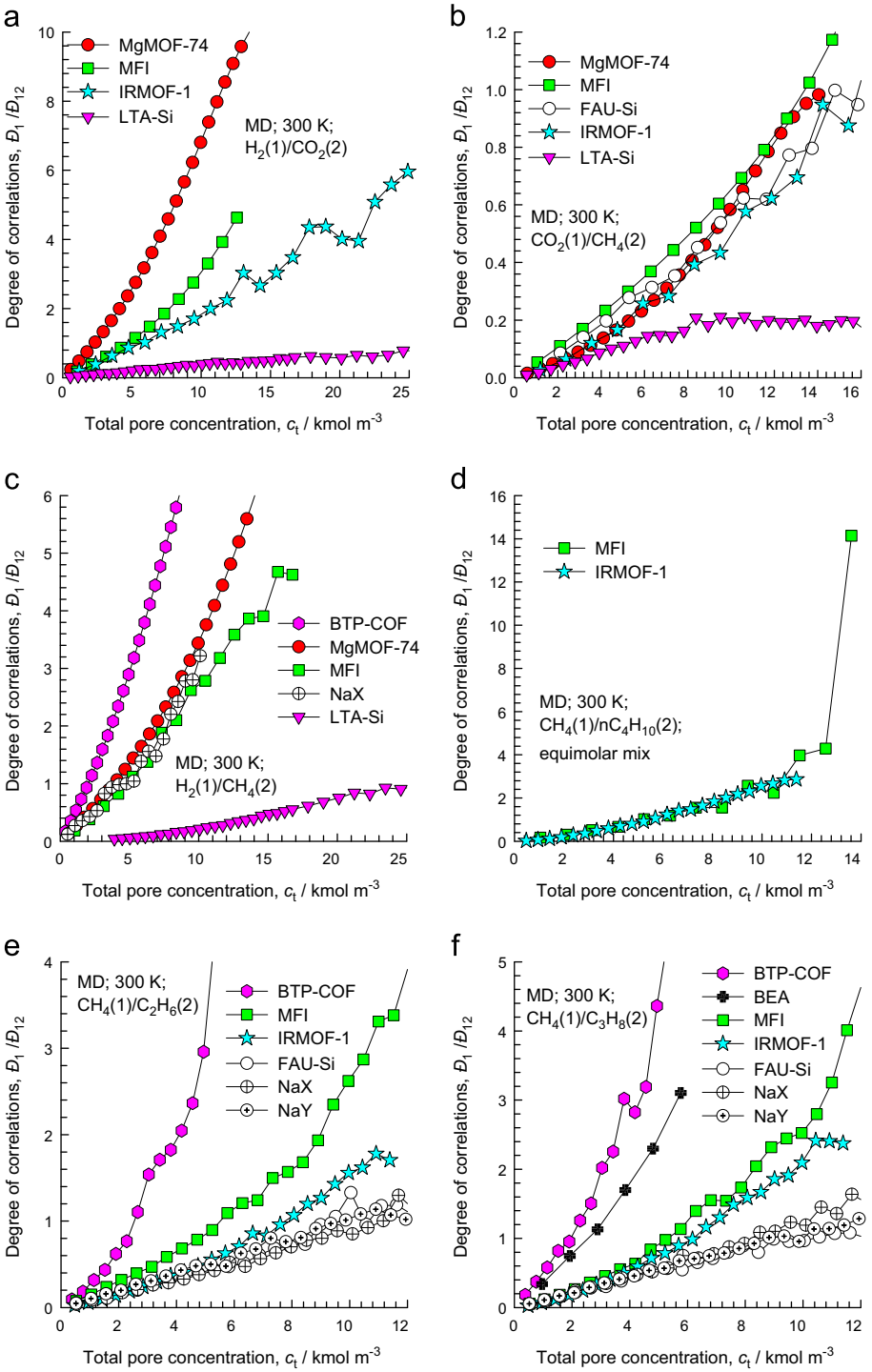

Fig. 3. MD simulation data for the degree of correlations, $Đ_1/Đ_{12}$, for diffusion of equimolar binary mixtures ($c_1=c_2$) (a) H_2/ CO_2, (b) CO_2/CH_4, (c) H_2/CH_4, (d) CH_4/nC_4H_{10}, (e) CH_4/C_2H_6, and (f) CH_4/C_3H_8 at 300 K in a variety of host materials, as a function of the total pore concentration, $c_t=(q_1+q_2)/V_p$. As explained in previous works, the comparisons of diffusivities in different host materials is best done in terms of pore concentrations, expressed in terms of the accessible pore volume V_p [20]. A more detailed data set on the $Đ_1/Đ_{12}$is provided as Supplementary Material.

CHA, DDR and LTA; the reason is that the molecules jump one-at-a-time across the narrow windows separating adjacent cages. To visualize the inter-cage hopping, video animations of the MD simulations for diffusion of H_2/CO_2 and CH_4/CO_2 mixtures in LTA zeolite is provided as Supplementary Material. These animations also clearly demonstrate that CO_2 molecules jump length-wise across the windows. At the other end of the spectrum, correlations are strongest in one-dimensional (1D) channel structures (e.g. NiMOF-74), intersecting channels (e.g. MFI), and "open" structures (e.g. IRMOF-1, FAU, NaX) consisting of large cages separated by wide windows.

3. Systems with negligible degree of correlations

We first examine mixture permeation across structures such as CHA, DDR, LTA, ITQ-29, SAPO-34, and ZIF-8 that consist of cages separated by narrow windows in the 3.2–4.2 Å range. We shall analyze experimental mixture permeation data to examine whether the uncoupled Eq. (8) is of sufficient accuracy for use in practice.

Consider permeation of CO_2/CH_4 separation using a membrane made up of thin layers of SAPO-34 that consists of 316 $Å^3$ sized cages separated by 3.8 Å × 4.2 Å sized windows. Experimental data on permeances Π_i of CO_2 and CH_4 determined from unary and binary permeation experiments are compared in Fig. 4a. We note that while the permeance of CO_2 in the mixture remains unchanged from that of the pure component, the permeance of CH_4 in the mixture is lower in the mixture than the pure component value. Consequently, the value of S_{perm} from mixture permeation experiments is higher than those determined from unary permeation; see Fig. 4b. The differences in the two sets S_{perm} values are primarily because the adsorption selectivity, S_{ads}, determined from IAST calculations, is significantly higher for mixture adsorption; Fig. 4b also indicates that the S_{perm} value is significantly higher than the corresponding value of S_{ads}. The rationale is that CO_2 molecules jump length-wise across the windows (see snapshot in Fig. 4c) and have a significantly higher diffusivity than that of CH_4; this is verified by molecular dynamics (MD) simulations for the structural analog CHA [22]. As stressed in the literature [22,23], kinetic diameters are insufficient indicators of the hierarchy of diffusivity values; molecular configurations, bond length and bond angles are also important determinants. Indeed, an important advantage of SAPO-34 in CO_2/CH_4 mixture separation is that the diffusion selectivity favors CO_2; S_{ads} and S_{diff} complement each other. Therefore, SAPO-34 membranes have significant potential for use in natural gas purification applications that operate at high pressures.

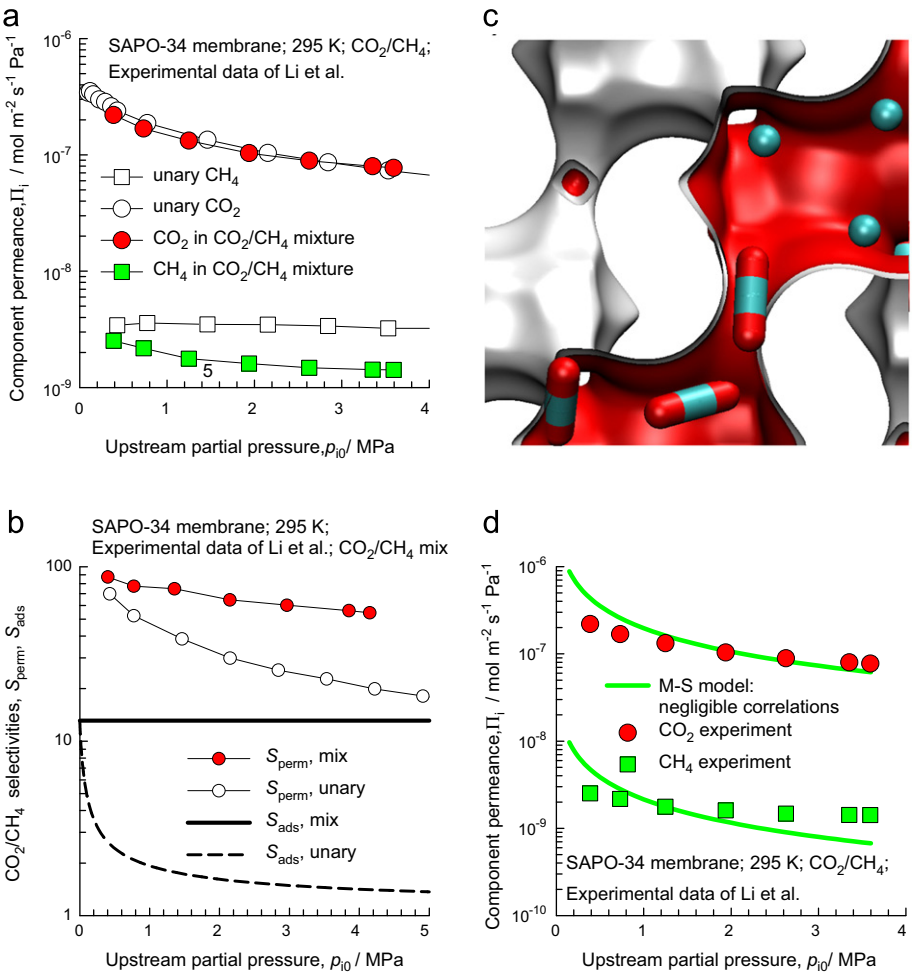

Fig. 4. (a) Permeances of CO_2 (1) and CH_4 (2) determined for unary and binary mixture permeation across SAPO-34 membrane [24–26]. (b) Comparison of S_{perm} and S_{ads} values for CO_2/CH_4 mixtures compared with corresponding values determined from unary experiments. (c) Snapshot, obtained from molecular simulation, showing adsorbed CO_2 and CH_4 molecules in SAPO-34. (d) Experimental data on permeances of CO_2 and CH_4 compared with the estimations of Eq. (8). The estimations are based on the values of $\rho Đ_1/\delta = 0.035$ kg m^{-2} s^{-1}, and $\rho Đ_2/\delta = 0.005$ kg m^{-2} s^{-1}, both determined from unary permeation data. Further details of the model calculations, including isotherm fits, are provided in the Supplementary Material.

We now attempt quantitative modeling of mixture permeation using uncoupled Eq. (8). For this purpose, the transport coefficients $\rho Đ_1/\delta$, and $\rho Đ_2/\delta$, are first determined from unary permeation experiments for conditions corresponding to the lowest upstream pressures. The values thus obtained are subsequently used in the Eq. (8) for estimation of N_i, and Π_i in the mixture. These estimations are in reasonable agreement with the experimental data; see Fig. 4d. More detailed modeling [24–26], accounting rigorously for the loading dependence of the M–S diffusivities, $Đ_1$ and $Đ_2$ leads to improved agreement between model calculations and experiment, but does not alter the conclusion that correlation effects are of negligible significance in this case and that $(Đ_1/Đ_{12})\to 0$ is a good assumption to make.

The interpretation of the experimental data on H_2/CO_2 separation with SAPO-34 membrane [26] is somewhat different in detail. The permeance of H_2 in the mixture is considerably lower, by about order of magnitude, than the unary permeance value; see Fig. 5a. This order-of-magnitude decrease in the permeance of H_2 is primarily attributable to the fact that the value of S_{ads} for mixture adsorption is about an order of magnitude higher than S_{ads} calculated from pure component isotherm data; see Fig. 5b. Another point to note is that the S_{perm} value is significantly lower than the corresponding value of S_{ads}; this is because S_{diff} favors the significantly smaller H_2 molecule. The S_{ads} and S_{diff} characteristics of H_2/CO_2 mixtures do not complement each other. SAPO-34 membrane is CO_2-selective because the adsorption favors CO_2 and overcomes the diffusional disadvantages. Calculations based on Eq. (8) result in reasonably good agreement with the mixture permeation experiments; see Fig. 5c. A more detailed modeling exercise, based on exact numerical solution of the M–S equations accounting rigorously for the loading dependence of the M–S diffusivities, is available in an earlier publication [26].

The 3.65 Å × 4.4 Å windows of DDR have a more oblong shaped aperture compared to that of SAPO-34. One important consequence is that the window regions of DDR are preferred locations for CO_2 molecules [27]; see snapshot in Fig. 6a. Experimental data [28,29] on component permeances across a DDR membrane shows that the Π_i values in the mixture are nearly the same as for pure components (cf. Fig. 6b and c), implying a negligible degree of correlations, i.e. $(Đ_1/Đ_{12})\to 0$. Rigorous modeling of the DDR permeation data also reveals that the preferential location of CO_2 at the window regions has the effect of hindering the inter-cage hopping of CH_4 [17,27,30]. One important consequence of such hindering is that the CO_2/CH_4 permeation selectivity with DDR is about 1000, which is significantly higher than that obtained with SAPO-34.

The size of the window aperture of ZIF-8 (see landscape in Fig. 7a) from crystallographic data is 3.26 Å, but the lattice framework flexibility is such that molecules as large as 2,2 dimethylbutane can be transported for one cage (approximately 1170 Å^3 in size) to an adjacent cage [23,31,32]. By contrast, lattice flexibility has little influence on the inter-cage hopping across narrow 8-ring windows of CHA, LTA, ITQ-29, SAPO-34, and DDR zeolites [33,34]. Experimental data for Π_i of CO_2 and CH_4 determined for unary and binary mixture permeation experiments [35] are shown in Fig. 7b. We note that the permeance of each component is the practically the same in the mixture as for the pure component, suggesting that diffusional coupling effects are of negligible importance. The lattice flexibility of ZIF-8 is most likely the reason that the CO_2/CH_4 permeation selectivity with ZIF-8 is only in the range of 2–4, significantly lower than S_{perm} values obtained with DDR and SAPO-34.

The transient uptake data of Li et al. [36] for ZIF-8 show propene diffusivity to be 125 times that of propane; the higher alkene diffusivity must be ascribed to subtle differences in bond lengths and bond angles [22,23]. This would suggest that ZIF-8 has the potential for diffusion-selective separation of propene/propane mixtures. This expectation is fulfilled by the data of Pan et al. [37] on propene/ propane permeances across a ZIF-8

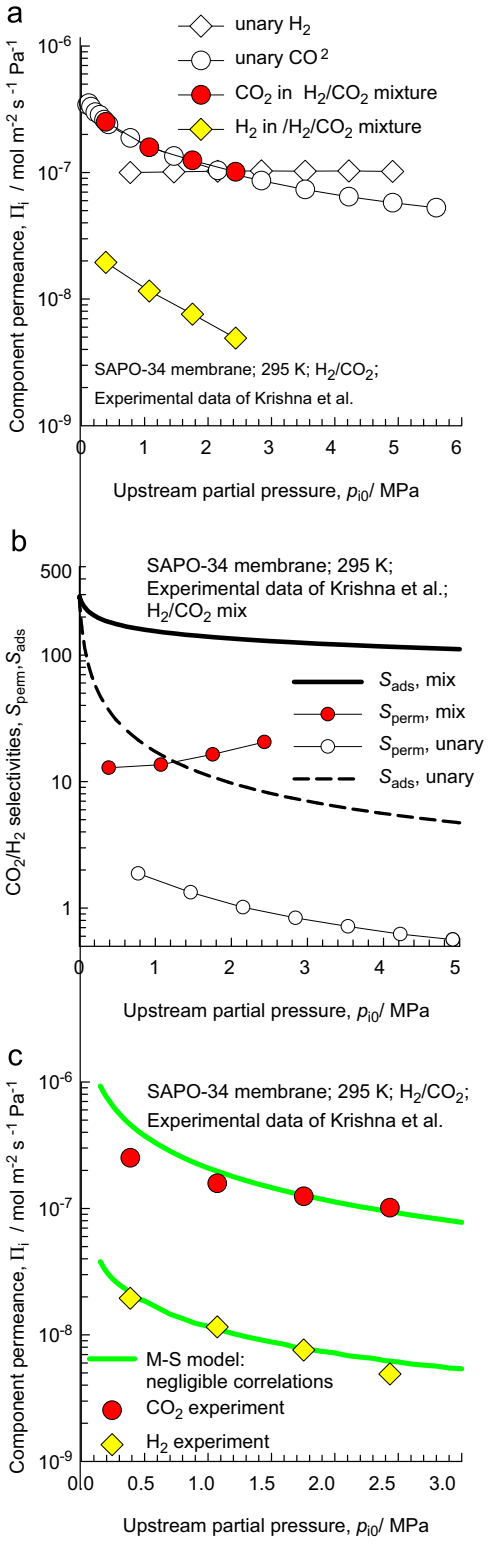

Fig. 5. (a) Permeances of H_2 (1) and CO_2 (2) determined for unary and binary mixture permeation across SAPO-34 membrane [26]. (b) Comparison of S_{perm} and S_{ads} values for H_2/CO_2 mixtures compared with corresponding unary values. (c) Experimental data on permeances of H_2 and CO_2 compared with the estimations of Eq. (8). The estimations are based on the values of the membrane transport coefficients $\rho Đ_1/\delta =$ 0.3kg m^{-2} s^{-1}, and $\rho Đ_2/\delta =$0.035 kg m^{-2} s^{-1}, both determined from unary permeation data. Further details of the model calculations, including isotherm fits, are provided in the Supplementary Material.

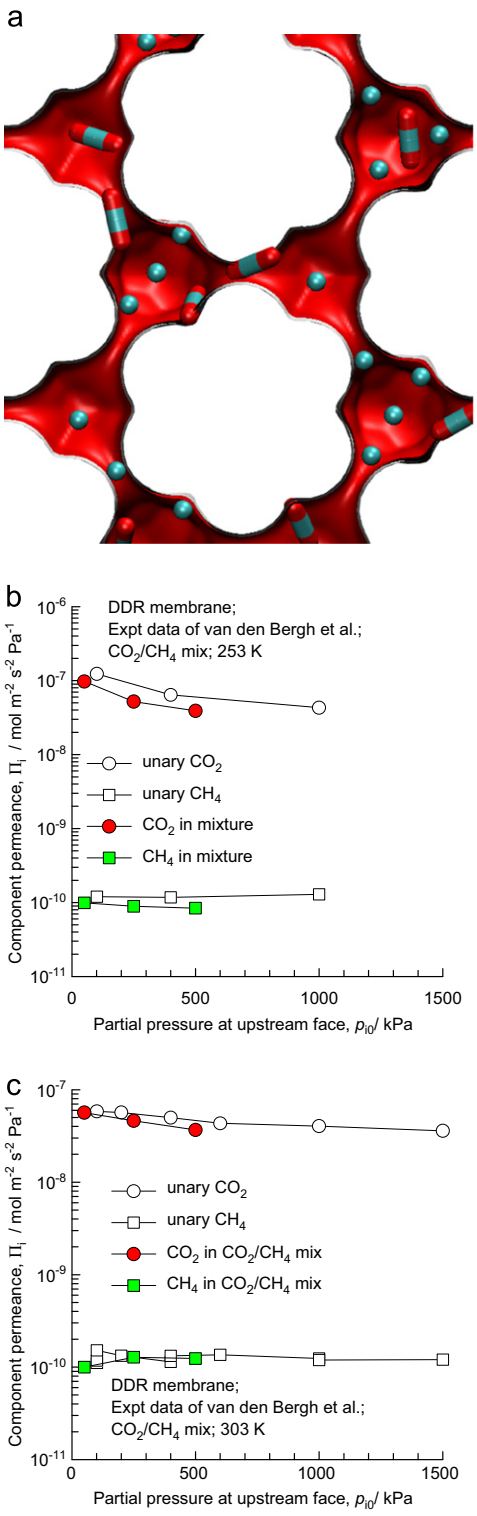

Fig. 6. (a) Snapshot, obtained from molecular simulation, showing adsorbed CO_2 and CH_4 molecules in DDR. (b, c) Permeances of CO_2 and CH_4 determined for unary and binary mixture permeation across DDR membrane at (b) 253 K, and (c) 303 K [28,29].

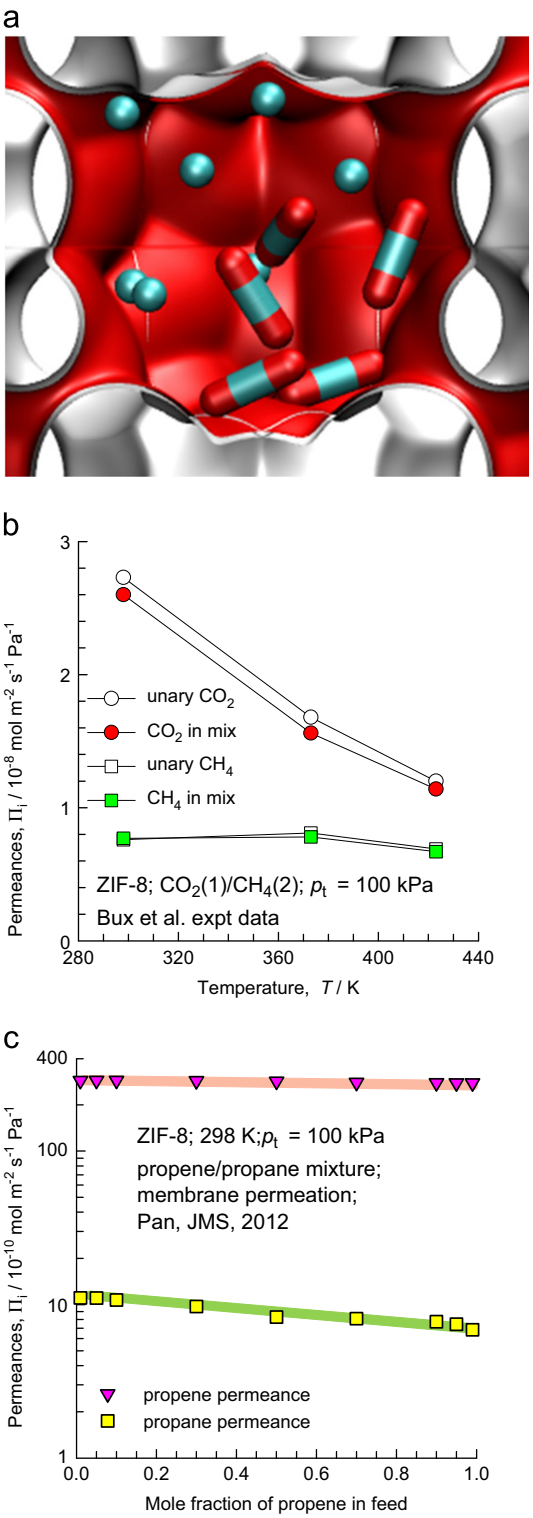

Fig. 7. (a) Snapshot, obtained from molecular simulation, showing adsorbed CO_2 and CH_4 molecules in the cages of ZIF-8. (b) Permeances of CO_2 and CH_4 determined for unary and binary mixture permeation by Bux et al. [35] with an upstream pressure of 100 kPa. (c) Permeances of propene and propane across a ZIF-8 membrane, determined as a function of the mole fraction of propene in the gas phase in the upstream compartment in the experiments reported by Pan et al. [37]. Further details on adsorption and diffusion are provided in the Supplementary Material.

membrane; see Fig. 7c. The magnitude of Π_i is hardly influenced by the mixture composition in the upstream compartment; this implies that correlation effects have negligible influences and Eq. (8) is of adequate accuracy. The value of S_{perm} is about 35, lower than the value of 125 anticipated from the uptake data of Li et al. [36]. The reason for the lower permeation selectivity is that the adsorption selectivity is in favor of the saturated propane [38].

Analogously, the membrane permeation experiments of Bux et al. [39] demonstrate that the permeation selectivity favors ethene; the rationale for this is traceable to the significantly

higher diffusivities of the unsaturated species, as determined from Infra-Red Microscopy measurements. A further confirmation of the subtle influence of bond lengths and bond angles on diffusivities of alkenes and alkanes is provided by Ruthven and Reyes [40] who report S_{diff} values for propene/propane mixtures in excess of 1000 for CHA and DDR zeolites.

4. Systems with significant degree of correlations

We now investigate membranes made up of thin layers of materials such as MFI, FAU, NaX, IRMOF-1, and Matrimid for which correlation effects exert a strong influence causing the mixture permeation characteristics to be significantly different from unary permeation. Such effects are best illustrated by considering the experimental data of Sandström et al. [41] for permeances of H_2 and CO_2 in a MFI membrane, determined both from unary and binary mixture permeation data; see Fig. 8a. We note that the permeance of the tardier CO_2 in the mixture is practically the same as that for unary permeation for the entire range of upstream (feed) partial pressures. For H_2, the permeance in the mixture is about an order of magnitude lower than from unary experiments. This implies that mixture permeation is CO_2-selective, whereas the data based on unary permeation demonstrates H_2-selective performance; see S_{perm} data in Fig. 8b. This

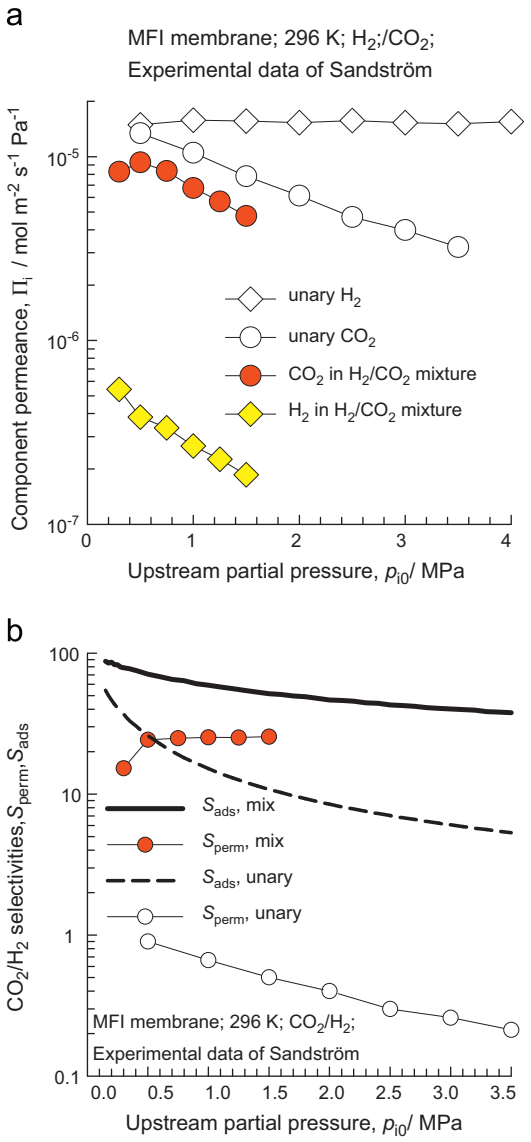

Fig. 8. (a) Permeances of H_2 and CO_2 determined for unary and binary mixture permeation across MFI membrane; data of Sandström et al. [41]. (b) Comparison of S_{perm} and S_{ads} values for CO_2/H_2 mixtures compared with corresponding unary values.

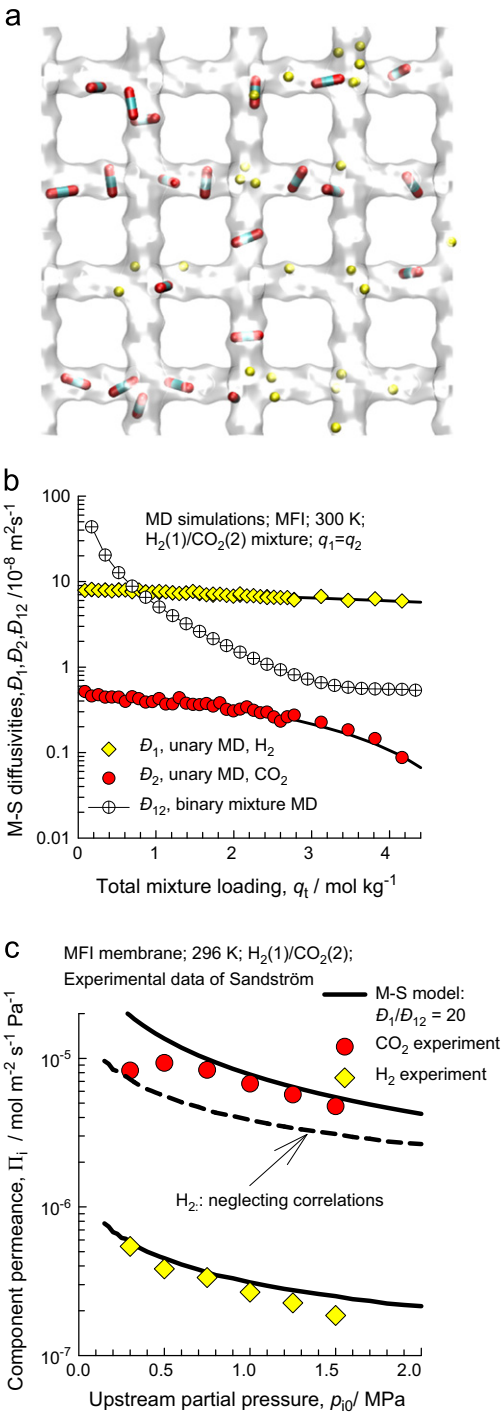

Fig. 9. (a) Snapshot showing the location of H_2 (1) and CO_2 (2) adsorbates within the intersecting channel structures of MFI. Video animations of the motion of the molecules is provided as Supplementary Material. (b) MD simulation data for $Đ_1$, $Đ_2$, and $Đ_{12}$ for diffusion of equimolar ($q_1=q_2$) H_2 (1)/CO_2 (2) mixtures in MFI as a function of the total mixture loading, q_t. (c) Experimental data on permeances of H_2 and CO_2 compared with the estimations of Eqs. (2) and (3). The estimations are based on the values of $\rho Đ_1/\delta = 80\ kg\ m^{-2}\ s^{-1}$, $\rho Đ_2/\delta = 2.7\ kg\ m^{-2}\ s^{-1}$, both determined from unary permeation data. Furthermore, the degree of correlations for H_2 is assumed to be $Đ_1/Đ_{12} = 20$. Further details of the model calculations, including isotherm fits, are provided in the Supplementary Material.

reversal of selectivity is only partly attributable to the fact that S_{ads} for mixture adsorption is much more strongly in favor of CO_2. For a proper modeling of the permeation experiments we need to have a clear understanding, and quantification, of correlation effects.

MFI zeolite consists of a set of intersecting channels of approximately 5.5 Å in size; Fig. 9a shows snapshot showing the location of H_2 and CO_2 adsorbates within the intersecting channels. The presence of strongly adsorbed CO_2 serves to hinder the motion of H_2; a qualitative appreciation of such hindering is evident by visual examination of the video animations of H_2/CO_2 mixture diffusion, uploaded as Supplementary Material. Indeed, Sandström et al. [41] consider the reduction in the H_2 permeance to be a result of "blocking" by the partner CO_2 molecules.

Fig. 9b presents MD simulation data for the M–S diffusivities, $Đ_1$, $Đ_2$, and $Đ_{12}$ for diffusion of equimolar H_2 (1)/CO_2 (2) mixtures in MFI as a function of the total mixture loading, q_t. In the experiments of Sandström et al. [41], the total mixture loadings q_t are in the range 2–4 mol kg^{-1}. In this range of loadings the MD data show $Đ_1/Đ_{12} \approx 10-20$, and $Đ_1/Đ_{12} \approx 0.5-1$. Calculations using Eqs. (2) and (3) taking $Đ_1/Đ_{12} = 20$, along with the values of $\rho Đ_1/\delta =$ 80 kg m^{-2} s^{-1} and $\rho Đ_2/\delta = 2.7$ kg m^{-2} s^{-1}, both determined from unary permeation data are shown in Fig. 9c. There is a good agreement of model calculations with the experimentally determined permeances. In order to underscore the significant influence of correlations, Fig. 9c also present the model calculations using Eq. (8) in which correlations are considered negligible. This simplified scenario over-estimates the H_2 permeance by about an order of magnitude; in sharp contrast, the simplified model predictions for CO_2 are indistinguishable from those obtained taking correlations into account. Generally speaking, correlation effects have a strong retarding influence of the permeation of more-mobile-less-strongly-adsorbed molecules. Conversely, correlation effects are of lesser importance for tardier-more-strongly-adsorbed species. Slowing-down effects cause of the decrease in the H_2/CO_2 selectivity of Matrimid membrane with increasing proportion of CO_2 in the upstream membrane compartment [42].

We now re-analyze the experimental data of van de Graaf et al. [9] for permeation of CH_4, C_2H_6, and C_3H_8 across an MFI membrane at 303 K. The values of the membrane transport coefficients $\rho Đ_i/\delta$ for each alkane are obtained from fitting the unary permeance data (cf. Fig. 10a). These values are used for estimations of the permeances in CH_4/C_2H_6, and CH_4/C_3H_8 mixtures. The two sets of experiment permeance data for CH_4/C_2H_6 mixtures carried out under equimolar feed mixtures (cf. Fig. 10b), and with varying feed composition (cf. Fig. 10c), can be described reasonably well taking $Đ_1/Đ_{12} = 1$; this value is within the range of values obtained from MD simulations presented in Fig. 3e,

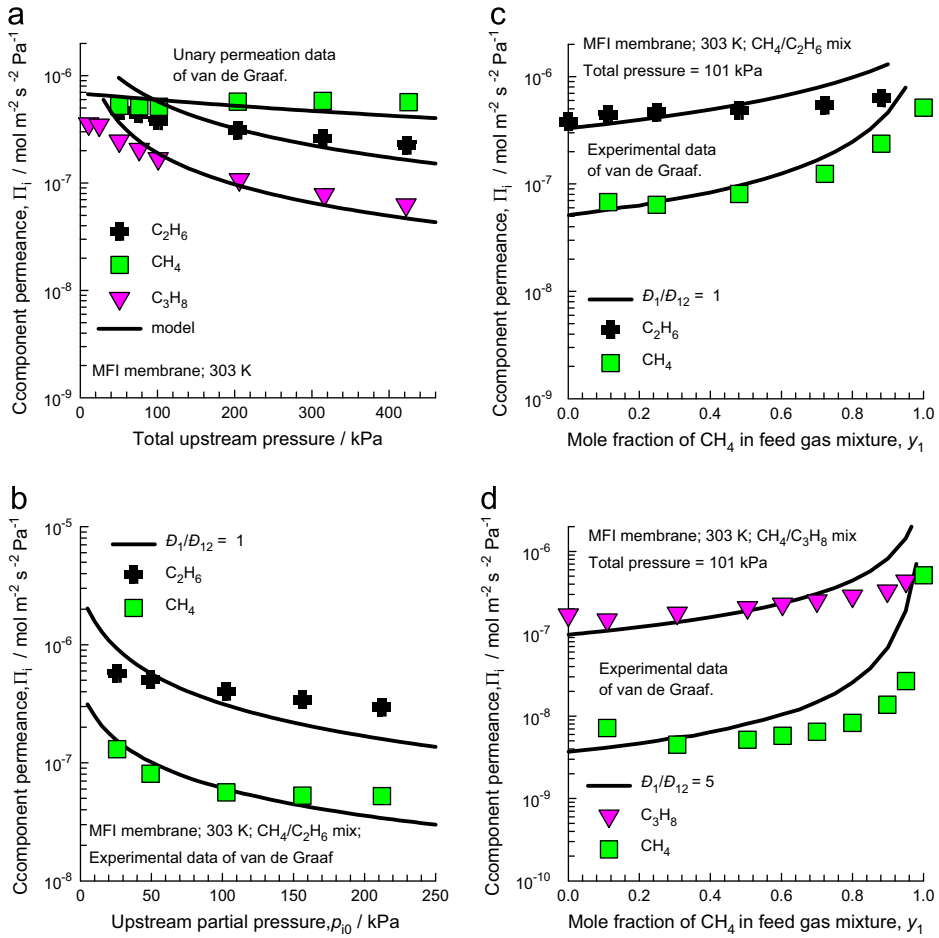

Fig. 10. (a) Experimental data of van de Graaf et al. [9] for unary permeances of CH_4, C_2H_6, and C_3H_8 across an MFI membrane at 303 K. The continuous solid lines represent model calculations with the values of the membrane transport coefficients $\rho Đ_1/\delta =$ 0.08 kg m^{-2} s^{-1}, 0.016 kg m^{-2} s^{-1}, and 0.005 kg m^{-2} s^{-1}, respectively; these values are used in the estimations of permeances in mixtures. (b, c) Experimental data for permeances of (b, c) CH_4/C_2H_6, and (d) CH_4/C_3H_8 mixtures. In (b) the upstream membrane compartment contains equimolar gas mixtures. In (c) and (d), the proportion of CH_4 in the feed compartment is varied, keeping the total pressure at 101 kPa. The continuous solid lines in (b), (c) and (d) are obtained using Eqs. (2) and (3) with the transport coefficient values as above, along with the value of the degree of correlations for CH_4: In (b) and (c) the degree of correlations $Đ_1/Đ_{12} = 1$, and $Đ_1/Đ_{12} = 5$ in (d). Further details of the model calculations, including isotherm fits, are provided in the Supplementary Material.

when determined at the experimental mixture loadings. For CH_4/C_3H_8 mixtures, the adsorbate loadings are higher because of the stronger adsorption of propane; consequently the degree of correlations is stronger (cf. Fig. 3f). The CH_4/C_3H_8 mixture permeances are reasonably well described by taking $Đ_1/Đ_{12}=5$; see comparisons of model calculations with experiments in Fig. 10d. It is encouraging to note that Eqs. (2) and (3) cover the essential features of mixture permeation, albeit with assumed inputs on values of $Đ_1/Đ_{12}$.

An important feature of MFI membrane separation of H_2/CO_2, CH_4/C_2H_6, and CH_4/C_3H_8 mixtures is that in all three cases the high degree of correlations within the intersecting channels serve to enhance the S_{perm} values which favor the more strongly adsorbed species in each case. Estimating the membrane performance by ignoring correlations and using the simplified Eq. (6) for S_{diff} will provide pessimistic estimates of membrane performance.

Let us now consider the influence of operating temperature, T, on mixture permeation characteristics. Vroon et al.[43] report data on permeation of CH_4/nC_4H_{10} mixtures in MFI membranes. Over the entire range of T, the permeance of nC_4H_{10} determined from mixture permeation is practically the same as for the pure component; see Fig. 11a. The situation with regard to the more mobile CH_4 is entirely different. At 298 K, the CH_4 permeance in the mixture is significantly lower, by a factor about 40, than that from unary permeation. As the temperature increases, the extent of lowering is considerably reduced, and at a temperature of 473 K, the lowering in CH_4 permeance is only about 20%. The rationale for this observation can be traced to the increase of the degree of correlations with increasing pore concentrations (cf. Fig. 3d); the pore concentrations are significantly lowered with increasing T.

Further evidence of the increasing importance of correlations with increasing pore concentrations is available in the experimental data of Bakker [44] for the permeation selectivity of CH_4/nC_4H_{10} mixtures in MFI membrane as a function of the upstream partial pressure of nC_4H_{10}, p_{20}; see Fig. 11b. While the model calculations assuming $Đ_1/Đ_{12}=5$, on basis of the data presented in Fig. 3d, is able to adequately capture the dependence of S_{perm} on p_{20}; neglecting correlations anticipates significantly lower selectivities; the deviations become larger with increasing proportion of nC_4H_{10}. This implies that slowing-down effects improve selectivities in favor of the tardier n-butane.

Another illustration of the increase in the significance of correlation effects with increasing proportion of the tardier species is provided by simulations of transient permeation of CH_4/C_3H_8 mixtures across MFI membrane with $p_{10}=95$ kPa, $p_{20}=5$ kPa. Fig. 11c shows the component fluxes calculated for the two scenarios, both including and neglecting correlation effects. In the initial phase, the pores of the membrane are predominantly occupied by the more mobile CH_4 molecule and the downstream compartment contains almost exclusively CH_4 molecules. With the ingress of the tardier C_3H_8 into the pores, slowing-down effects

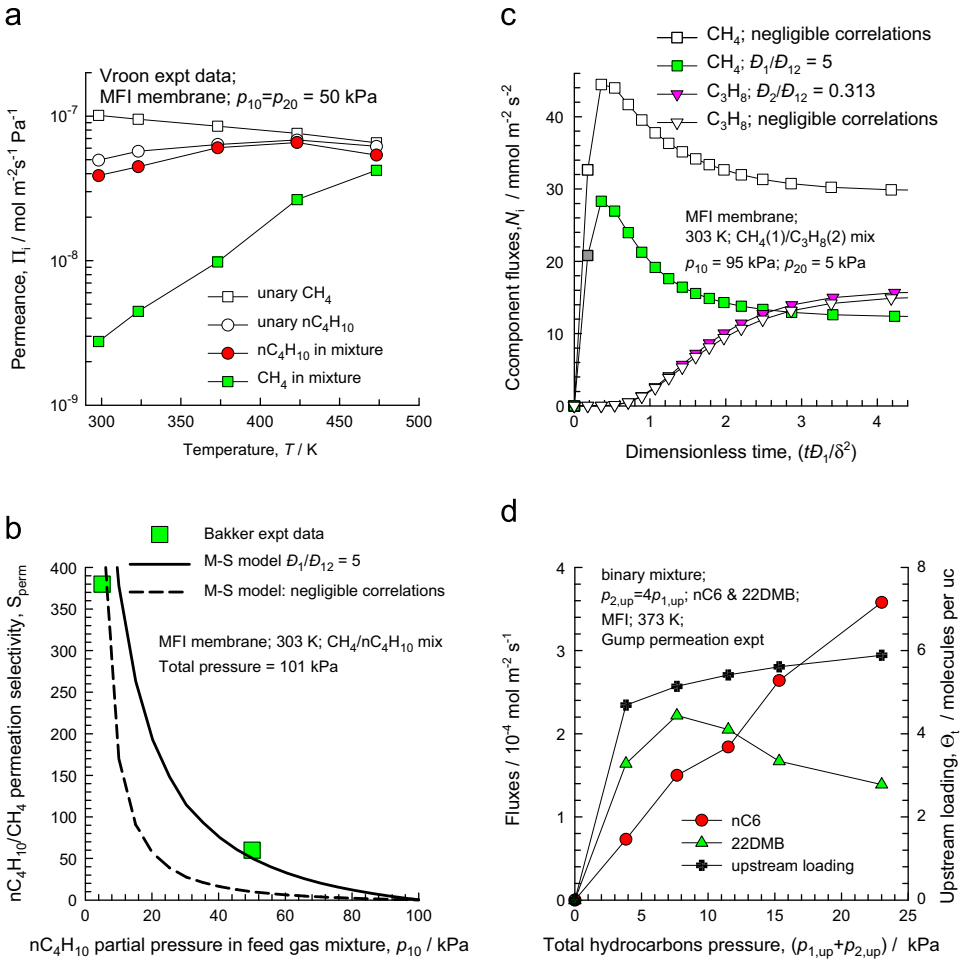

Fig. 11. (a) Component permeances for CH_4/nC_4H_{10} mixtures in MFI membranes as a function of the operating temperature; the experimental data are from Vroon et al. [43]. (b) Permeation selectivity of CH_4/nC_4H_{10} mixtures in MFI membrane as a function of the upstream partial pressure of nC_4H_{10}. (c) Transient permeation of CH_4/C_3H_8 mixtures across MFI membrane with $p_{10}=95$ kPa, $p_{20}=5$ kPa. The simulation results are for the two scenarios: including correlations (with data inputs the same as used in Fig. 10d), and ignoring correlations. (d) Experimental data for nC6-22DMB binary mixture permeation across MFI membrane, with upstream partial pressures $f_2=4f_1$ [46].

come into play and the CH_4 flux suffers a reduction with increasing C_3H_8 ingress. Use of Eq. (8) predicts that the flux of CH_4 remains higher than that of C_3H_8 till steady-state is reached. Taking into account of correlations, results in the steady-state flux being lower than that of C_3H_8, in conformity with the experimental data shown in Fig. 10d. Experimental evidence of the curious maximum in the transient flux of the more mobile partner species is provided by Bakker [44] for MFI permeation.

Branched and cyclic hydrocarbons locate preferentially at the intersections of the channel structures of MFI zeolite [45]. There are four intersection sites per unit cell of MFI zeolites, and as a consequence the pure component isotherms of branched and cyclic hydrocarbons exhibit strong inflection characteristics at a loading, $\Theta = 4$ molecules per unit cell. Linear alkanes, on the other hand, can locate anywhere along the channels. The preferential location of branched alkanes at the intersections of MFI leads to other unusual adsorption and diffusion phenomena that can be exploited to achieve separation of hydrocarbon isomers [45]. For loadings $\Theta_t > 4$ molecules per unit cell, the adsorption is strongly in favor of the linear alkanes. For permeation of *n*-hexane(*n*C6)/2,2 dimethylbutane (22DMB) mixtures across an MFI membrane, the flux of 22DMB decreases when the upstream hydrocarbons pressures $p_t > 2$ kPa as observed in one set of the experiments of Gump et al. [46]; see Fig. 11d. At $p_t \approx 2$ kPa, the total loading in the zeolite ≈ 4 molecules per unit cell, and all the intersection sites are fully occupied and no more 22DMB can be adsorbed, causing the curious maximum in the 22DMB flux.

We believe that the proper appreciation, and quantification, of correlation effects can lead to the optimum choice of membrane materials. To demonstrate this, we consider separation of H_2/CO_2 and CH_4/CO_2 mixtures using NiMOF-74 membranes, that has been recently prepared using a layer-by-layer seeding technique [47]. NiMOF-74 has 1D hexagonal-shaped channels of 11 Å size (cf. Fig. 12a). From the unary permeance data at an upstream pressure of 0.1 MPa, the S_{perm} values for H_2/CO_2 mixture is 9.1, leading Lee et al. [47] to conclude: "high H_2/CO_2 ideal selectivity can be obtained for NiMOF-74 membranes". We shall demonstrate that an analysis of permeation of H_2/CO_2 mixtures across NiMOF-74 will lead us to entirely different conclusions due to a combination of two separate factors: (1) the mixture adsorption being strongly in favor of CO_2 by a factor of 100–500 (see IAST calculation data for S_{ads} in Figs. 12b) and (2) strong correlation effects within the 1D channels will have the effect of slowing-down the considerably more mobile H_2. Estimation of S_{perm} assuming the value of $Đ_1/Đ_{12} = 20$, based on the MD simulation data for the structural analog MgMOF-74 with same channel size (cf. Fig. 3a) are shown in Fig. 12b. We note that the permeation selectivity is strongly in favor of CO_2, by a factor of 2–10, depending on the upstream pressure. If correlation effects are completely ignored, and the uncoupled Eq. (8) are used, then the separations are indeed H_2-selective as concluded by Lee et al. [47]. Experimental verifications of our predictions are warranted, in view of significantly higher permeabilities of NiMOF-74 membranes, by about two orders of magnitude, than materials such as ZIF-8, SAPO-34, and DDR [18].

CO_2-selective membranes having high permeabilities are particularly attractive in natural gas purification processes that operate on an extremely large scale at pressures ranging to 6 MPa. The unary permeance data for NiMOF-74 of Lee et al. [47] indicate that the selectivity is favor of CH_4 by a factor of 3.1. The lower permeance of CO_2 is caused primarily due its lower diffusivity within the channels caused by its higher binding energy [22]. However, our predictions of CH_4/CO_2 mixture permeation (cf. Fig. 12c) shows that the selectivities favor CO_2 by a factor of about 20. This selectivity is somewhat lower than that achieved with SAPO-34 (cf. Fig. 4b), but outweighing this is the significantly higher permeability in NiMOF-74 that is desirable in practice. For the same reason, membranes made of M-MOF-74 (M=Mg, Fe, Co, Ni, Zn) are attractive for alkene/alkene separations [48], affording high permeation selectivities favoring the unsaturated species.

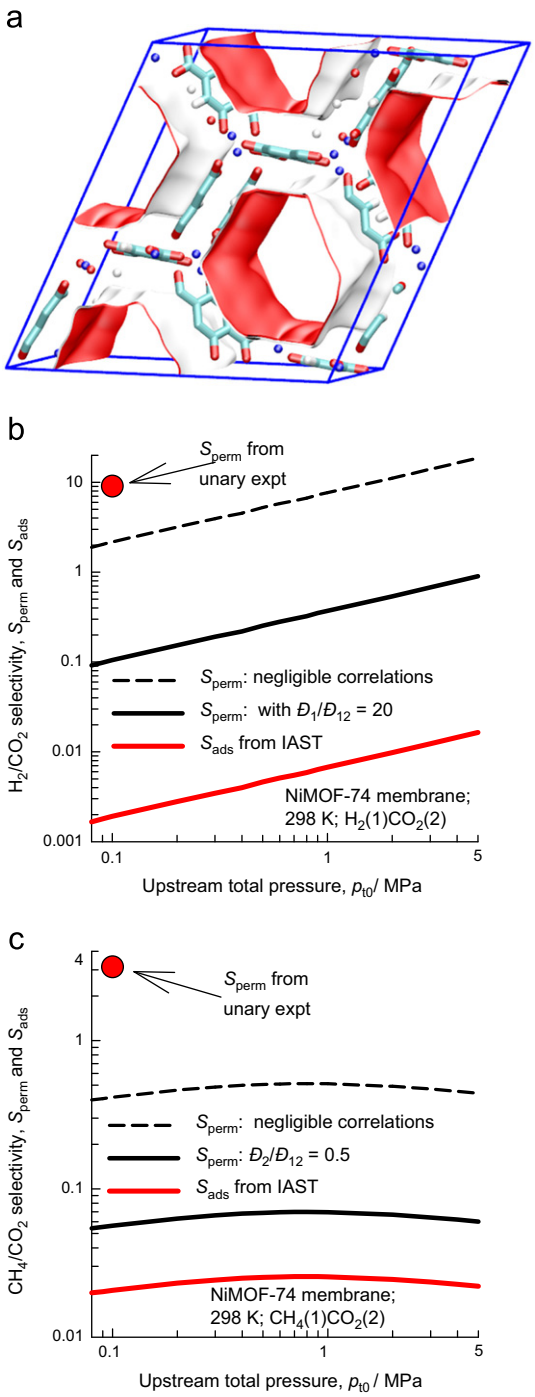

Fig. 12. (a) Pore landscapes showing the 1D hexagonal-shaped channels of NiMOF-74. (b) Comparison of H_2/CO_2 S_{perm} values determined from the unary permeance experiments of Lee et al. [47] with the estimations of Eqs. (2) and (3) for mixture permeation. (c) Comparison of CH_4/CO_2 S_{perm} values determined from the unary permeance experiments of Lee et al. [47] with the estimations of Eqs. (2) and (3) for mixture permeation. The estimations in (b) and (c) are based on the membrane transport coefficients for H_2, CH_4, and CO_2 of $\rho Đ_i/\delta =$ 17 kg m^{-2} s^{-1} and 0.3 kg m^{-2} s^{-1}. Also shown in (b) and (c) are IAST calculations of S_{ads}. Further details of the model calculations, including isotherm fits, are provided in the Supplementary Material.

5. Systems exhibiting molecular clustering

Pervaporation of water/alcohol mixtures is an important process in the processing industry, and a wide variety of membrane materials has been used, including polymeric (e.g. PERVAP, Chitosan, PDMS), zeolites (e.g. CHA, LTA, MFI, FAU, DDR), zeolitic imidazolate frameworks (e.g. ZIF-8) and mixed matrix membranes [49–51]. There is considerable evidence in the literature to indicate that hydrogen bonding, and consequent cluster formation manifests in LTA-4A [52,53], MFI [54–64], ZIF-8 [65], Nafion [66], PDMS [67], NaX [68–72], and Chitosan [73].

For water/alcohol mixture diffusion, the diffusivity of each component is lowered due to molecular clusters being formed as a consequence of hydrogen bonding. This is illustrated in Fig. 13 that present MD simulations of $Đ_1$, and $Đ_2$ for water/alcohol mixture diffusion in FAU, MFI, LTA, DDR, and CHA zeolites. In all cases, the diffusivity of water is reduced with increasing proportion of alcohol. Hydrogen bonding between water and alcohol molecule pairs serves to act as a "flexible leash" linking the

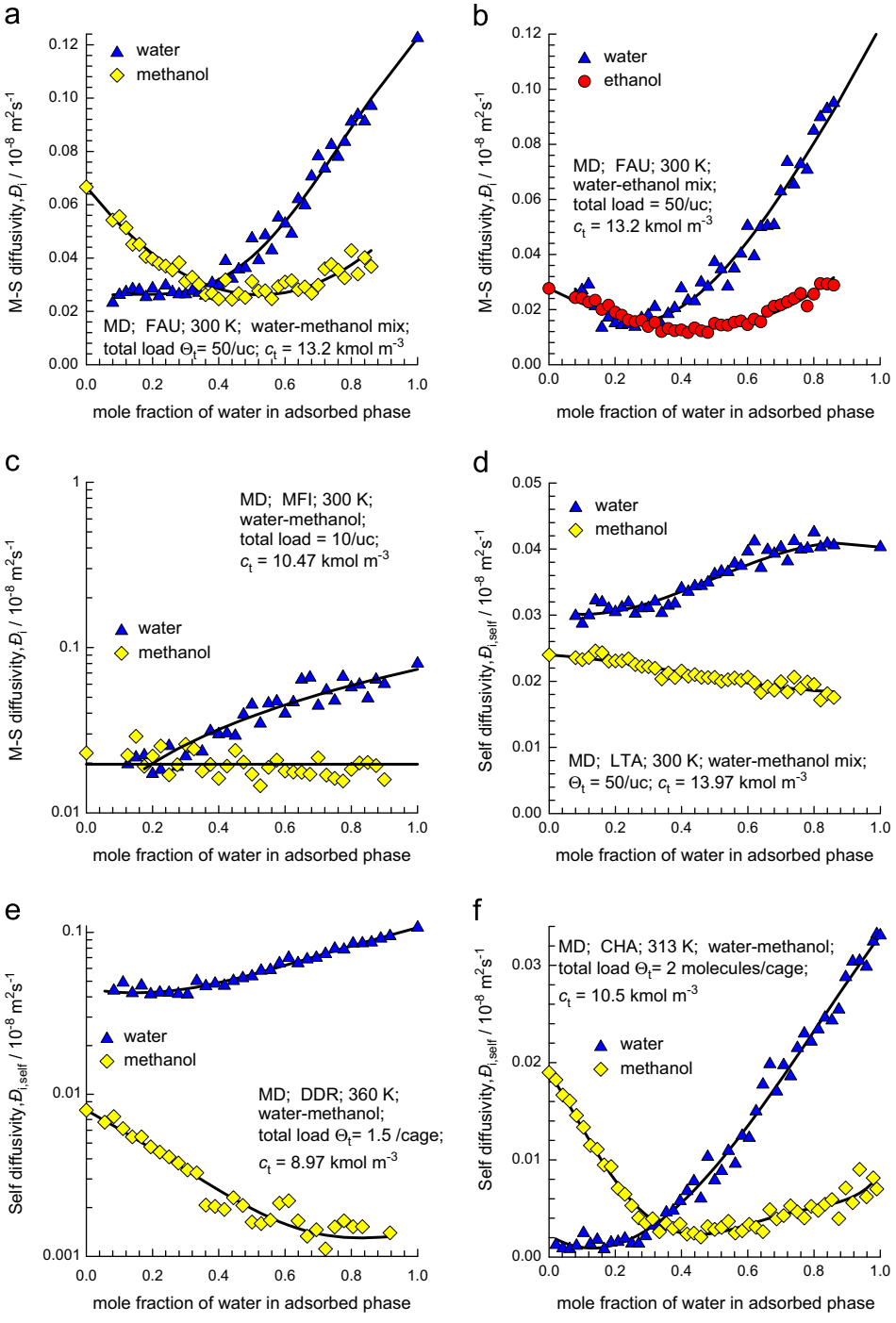

Fig. 13. Maxwell–Stefan diffusivities, $Đ_i$, in water/methanol, and water/ethanol mixtures of varying composition in (a, b) FAU, (c) MFI, (d) LTA, (e) DDR, and (f) CHA zeolites. The data are compiled from MD simulation results published in the literature [92–94]. In all cases the MD simulations were carried out under conditions in which the total concentration within the pores, c_t, is held constant; the values c_t are specified in each case and are based on the accessible pore volume in the various zeolites. In some cases the corresponding loadings per unit, Θ_t, are also specified. For CHA, DDR, and LTA the plotted diffusivities are the self-diffusivities, $D_{i,\,self}$, that are more accurate to determine and provide good approximations of the M–S diffusivities, i.e. $D_{i,\,self} \approx Đ_i$. The MD data are culled from our previous publications [92–97].

motion of the more mobile (water) and tardier (alcohol) species. The net result is that the motion of water is retarded due to cluster formation. For MFI, the diffusivity of methanol is practically independent of composition, while that for water shows a dramatic decrease with increasing methanol concentration (cf. Fig. 13c); this trend is the same as determined in the NMR experiments data of Caro et al. [74]. For LTA, and DDR the $D_{i,\ self}$ of methanol decreases with increasing proportion of water; see Fig. 13d and e. For CHA, the self-diffusivities for methanol show a decreasing trend for low water concentrations, until a minimum is reached; see Fig. 13f. A similar minimum in the alcohol self-diffusivity is observed for FAU zeolite; see Fig. 13a, and b. The general conclusion to be drawn from the MD data in Fig. 13 is that at either ends of the composition range, there is slowing-down of either component, due to increasing proportion of its partner species.

The clearest evidence of the strong influence of hydrogen bonding on diffusivities is demonstrated by comparing the experimental data [75] for the diffusivity of water in *n*-alkanes with those in *n*-alcohols of the same chain length; see Fig. 14a. We note that the diffusivity in the *n*-alcohols is lower by an order of magnitude. A part of this lowering is attributable to the higher alcohol viscosities but the major reduction is caused by hydrogen bonding.

A number of experimental data on pervaporation of water/alcohol, mixtures can be interpreted using the MD data presented in Fig. 13. In the discussions of their Chitosan pervaporation experimental results (plotted in Fig. 14b), Srinivasa Rao et al. [73] remark "The hydrogen bond interaction between water and ethylene glycol forms a cluster, which has the formula $(ROH)_x \cdot yH_2O$, so that separation by a hydrophobic membrane is difficult due to the relatively large coupling of the diffusion." The increase in the water diffusivity with increasing feed concentration of water, evident from the experimental data of Srinivasa Rao et al. [73], is similar to that observed in Fig. 13 for FAU. For water/isobutanol transport across PERVAP membranes, we note also that Valentínyi et al. [76] have adopted a diffusivity model in which the water diffusivity is an exponential function of the mole fraction of water in the feed mixture. For transport across a Nafion membrane in methanol fuel cell applications, strong hydrogen bonding between water and methanol is evidenced by molecular simulations [66], and NMR data on self-diffusivities in water/methanol mixtures provide further experimental confirmation of mutual slowing-down effects [77].

The experimental data of Khajavi et al. [78] for water–alcohol permeation across an H-SOD membrane show a significant increase in the water flux with increasing water concentrations in the feed mixture (see Fig. 14c), suggesting an increase in the water diffusivity with increasing proportion of water in the feed mixture.

For water/alcohol pervaporation across CHA zeolite membrane, the experimental data of Hasegawa et al. [79] show that the alcohol fluxes decrease with increasing water composition in the feed. Indeed, both water and alcohol fluxes are reduced with increasing concentrations of partner species in the mixture. Similar experimental data for water/alcohol pervaporation across DDR membranes are reported [80]. The decrease in the alcohol fluxes with increasing water concentration in the feed mixture

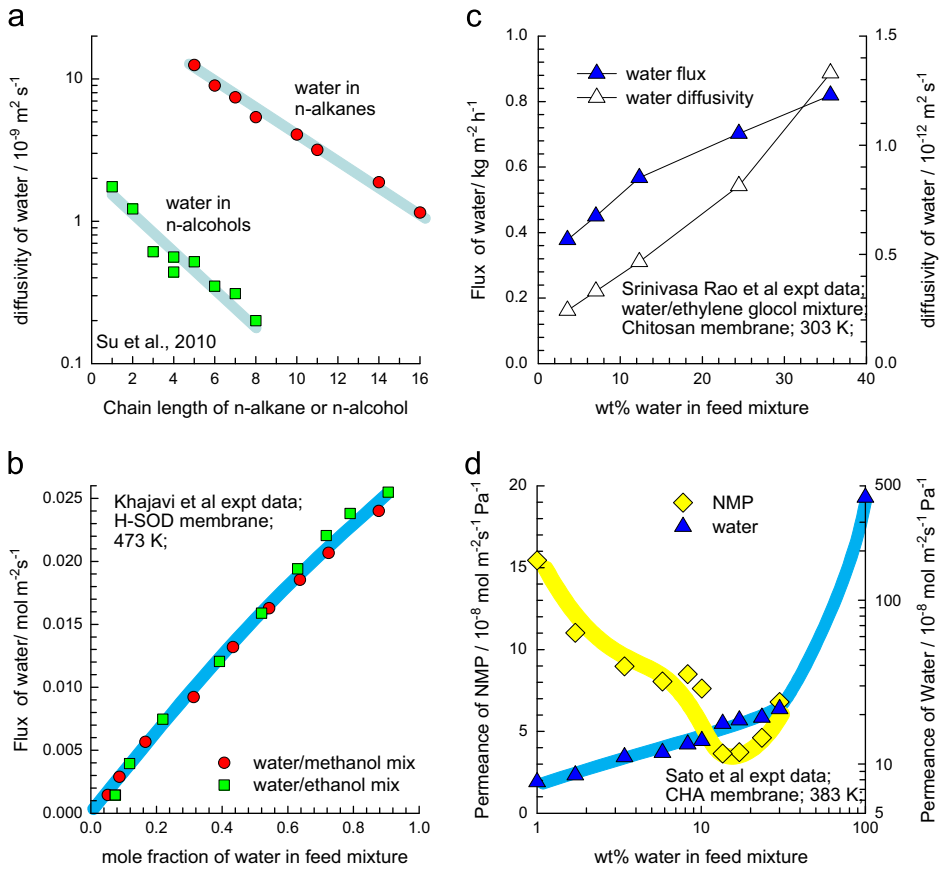

Fig. 14. (a) Comparison of the diffusivity of water in *n*-alkanes with those in *n*-alcohols of the same chain length; experimental data from Su et al. [75]. (b) Experimental data of Khajavi et al. [78] for water flux across a H-SOD membrane as a function of the water mole fraction in water/methanol, and water/ethanol mixtures. (c) Influence of wt% water in feed mixture on permeation flux, and diffusivity of water across Chitosan membrane; experimental data from Srinivasa Rao et al. [73]. (d) Experimental data of Sato et al. [51] for permeances for water/NMP pervaporation across CHA membrane.

observed experimentally in the CHA pervaporation experiments, must be ascribed, in part at least, to a reduction in the alcohol diffusivities observed in the MD simulation results presented in Fig. 13f.

The somewhat more complex dependence of the alcohol diffusivity on mixture composition observed in Fig. 13f is verified in the experimental data of Sato et al. [51] for industrial scale water/NMP pervaporation across CHA membrane. The NMP permeance decreases for water concentrations <10 wt%, and tends to increase when the water feed concentrations >15 wt%; see Fig. 14d. Since permeances are closely related to the diffusivities, the NMP diffusivities either decrease or increase depending on the feed composition.

An important consequence of molecular clustering is that the transport coefficients $\rho Đ_1/\delta$, and $\rho Đ_2/\delta$, cannot be estimated on the basis of unary pervaporation data. Furthermore, mutual slowing-down effects cannot be captured by the choice of $Đ_{12}$. In the study by Kuhn et al. [80] for water/alcohols pervaporation across a DDR membrane, it was found that the use of uncoupled Eq. (8) with the $Đ_1$, and $Đ_2$ determined from unary permeation data, lead to a severe overestimation of the permeation fluxes. Molecular simulations have demonstrated cluster formation for acetone/methanol mixtures [81], and this rationalizes finding of Yu et al. [82] that their experimental data on permeation of this mixture across an MFI membrane can only be rationalized if both the components $Đ_i$, are lowered when compared to the unary permeation values.

Mutual slowing-down effects have been commonly ignored in the published Maxwell–Stefan model implementations for mixture transport in water–alcohols pervaporation across DDR [80], LTA [11], MFI [82], methylated silica [83,84] membranes, and in methanol fuel cells [85,86]. Further research is necessary to generalize the Maxwell–Stefan formulation in a manner that explicitly allows for cluster formation, by defining a cluster to be a pseudo-species in the mixture. A step in this direction has been taken by Nasiri and Aroujalian [67] who model water/ethanol pervaporation across PDMS membrane by explicitly allowing for dimer formation.

6. Conclusions

By analyzing experimental data on permeation of a variety of mixtures across membrane materials with different characteristics we have discerned two types of coupling effects.

The first type of coupling occurs when the less-mobile species slows down its more mobile partner by not vacating an adsorption site quick for its more mobile partner to occupy that position. The Maxwell–Stefan formulation for mixture permeation, expressed in Eqs. (2) and (3), allows a quantitative prediction of mixture permeation using unary permeance data for estimation of the two membrane transport coefficients $\rho Đ_1/\delta$, and $\rho Đ_2/\delta$. The parameter $Đ_1/Đ_{12}$ quantifies the slowing-down effects; this parameter must be estimated on the basis of MD data. The degree of correlations, $Đ_1/Đ_{12}$, is strongly dependent on the pore size, topology and connectivity. In cage-type structures (e.g. CHA, DDR, LTA, and ZIF-8) in which adjacent cages are separated by narrow windows, correlation effects are weak. On the other hand the extent of correlations is particularly strong in structures consisting of one-dimensional channels (e.g. NiMOF-74), or intersecting channels (e.g. MFI) structures. Our work demonstrates the possibility of enhancing permeation selectivities by appropriate choice of materials with high degree of correlations. For example, the efficacy of NiMOF-74 membranes in natural gas purification applications hinges on the high degree of correlations within the 1D channels.

The second type of coupling occurs as a consequence of molecular clustering due to hydrogen bonding. Such clustering effects, commonly prevalent in alcohol/water pervaporation, can cause mutual slowing-down of partner molecules in the mixture. A priori predictions of mixture permeation is not possible on the basis of unary permeation data alone. In view of the significant importance of membrane pervaporation processes, there is a need to develop better understanding and models to describe the influence of molecular clustering on both mixture adsorption and diffusion.

Notation

c_i	pore concentration of species i, $c_i=q_i/V_p$, mol m^{-3}
c_t	total pore concentration in mixture, $c_t=q_t/V_p$, mol m^{-3}
$Đ_i$	M–S diffusivity of species i, m^2 s^{-1}
$D_{i,\text{self}}$	Self-diffusivity of species i, m^2 s^{-1}
$Đ_{12}$	M–S exchange coefficient, m^2 s^{-1}
F	factor defined by Eq. (9), dimensionless
p_i	partial pressure of species i in upstream compartment, Pa
p_t	total pressure in upstream compartment, Pa
q_i	molar loading of species i, mol kg^{-1}
q_t	total molar loading of mixture, mol kg^{-1}
N_i	molar flux of species i defined in terms of the membrane area, mol m^{-2} s^{-1}
S_{ads}	adsorption selectivity defined by Eq. (5), dimensionless
S_{diff}	diffusion selectivity defined by Eq. (6), dimensionless
S_{perm}	permeation selectivity defined by Eq. (1), dimensionless
T	temperature, K
V_p	pore volume, m^3 kg^{-1}
x_i	mole fraction of species i in the adsorbed phase, dimensionless

Greek letters

δ	thickness of membrane, m
Π_i	permeance of species i in mixture, mol m^{-2} s^{-1} Pa^{-1}
ϕ	fractional pore volume of microporous material, dimensionless
Θ_t	total molar loading of mixture, molecules per unit cell or per cage
ρ	framework density, kg m^{-3}

Subscripts

0	referring to upstream membrane compartment
i	referring to component i
t	referring to total mixture
δ	referring to downstream membrane compartment

Appendix A. Supporting information

Supplementary data associated with this article can be found in the online version at http://dx.doi.org/10.1016/j.memsci.2012.12.004.

References

[1] M. Anderson, H. Wang, Y.S. Lin, Inorganic membranes for carbon dioxide and nitrogen separation, Rev. Chem. Eng. 28 (2010) 101–121.
[2] J. Caro, Are MOF membranes better in gas separation than those made of zeolites? Curr. Opin. Chem. Eng. 1 (2011) 77–83.
[3] E. Favre, Membrane processes and postcombustion carbon dioxide capture: challenges and prospects, Chem. Eng. J. 171 (2011) 782–793.

[4] J. Gascon, F. Kapteijn, Metal-organic framework membranes—high potential, bright future? Angew. Chem. Int. Ed. 49 (2010) 1530–1532.
[5] J. Kärger, D.M. Ruthven, D.N. Theodorou, Diffusion in Nanoporous Materials, Wiley – VCH, Weinheim, 2012.
[6] R. Krishna, J.M. van Baten, In silico screening of zeolite membranes for CO_2 capture, J. Membr. Sci. 360 (2010) 323–333.
[7] R. Krishna, J.M. van Baten, In silico screening of metal-organic frameworks in separation applications, Phys. Chem. Chem. Phys. 13 (2011) 10593–10616.
[8] M. Yu, R.D. Noble, J.L. Falconer, Zeolite membranes: microstructure characterization and permeation mechanisms, Acc. Chem. Res. 44 (2011) 1196–1206.
[9] J.M. van de Graaf, F. Kapteijn, J.A. Moulijn, Modeling permeation of binary mixtures through zeolite membranes, AIChE J. 45 (1999) 497–511.
[10] W. Zhu, P. Hrabanek, L. Gora, F. Kapteijn, J.A. Moulijn, Role of adsorption in the permeation of CH_4 and CO_2 through a silicalite-1 membrane, Ind. Eng. Chem. Res. 45 (2006) 767–776.
[11] M. Pera-Titus, C. Fité, V. Sebastián, E. Lorente, J. Llorens, F. Cunill, Modeling pervaporation of ethanol/water mixtures within 'real' zeolite NaA membranes, Ind. Eng. Chem. Res. 47 (2008) 3213–3224.
[12] J. Sublet, M. Pera-Titus, N. Guilhaume, D. Farrusseng, L. Schrive, P. Chanaud, B. Siret, S. Durécu, Technico-economical assessment of MFI-type zeolite membranes for CO_2 capture from post-combustion flue gases, AIChE J. 58 (2012) 3183–3194.
[13] R. Krishna, Describing the diffusion of guest molecules inside porous structures, J. Phys. Chem. C 113 (2009) 19756–19781.
[14] R. Krishna, Diffusion in porous crystalline materials, Chem. Soc. Rev. 41 (2012) 3099–3118.
[15] A.L. Myers, J.M. Prausnitz, Thermodynamics of mixed gas adsorption, AIChE J. 11 (1965) 121–130.
[16] R. Krishna, J.M. van Baten, Insights into diffusion of gases in zeolites gained from molecular dynamics simulations, Micropor. Mesopor. Mater. 109 (2008) 91–108.
[17] R. Krishna, J.M. van Baten, Onsager coefficients for binary mixture diffusion in nanopores, Chem. Eng. Sci. 63 (2008) 3120–3140.
[18] R. Krishna, J.M. van Baten, Investigating the potential of MgMOF-74 membranes for CO_2 capture, J. Membr. Sci 377 (2011) 249–260.
[19] R. Krishna, J.M. van Baten, Maxwell–Stefan modeling of slowing-down effects in mixed gas permeation across porous membranes, J. Membr. Sci. 383 (2011) 289–300.
[20] R. Krishna, J.M. van Baten, Unified Maxwell–Stefan description of binary mixture diffusion in micro- and meso- porous materials, Chem. Eng. Sci 64 (2009) 3159–3178.
[21] B.E. Poling, J.M. Prausnitz, J.P. O'Connell, The Properties of Gases and Liquids, 5th edition, McGraw-Hill, New York, 2001.
[22] R. Krishna, J.M. van Baten, Investigating the relative influences of molecular dimensions and binding energies on diffusivities of guest species inside nanoporous crystalline materials, J. Phys. Chem. C 116 (2012) 23556–23568.
[23] C. Zhang, R.P. Lively, K. Zhang, J.R. Johnson, O. Karvan, W.J. Koros, Unexpected molecular sieving properties of zeolitic imidazolate framework-8, J. Phys. Chem. Lett. 3 (2012) 2130–2134.
[24] S. Li, J.L. Falconer, R.D. Noble, R. Krishna, Modeling permeation of CO_2/CH_4, CO_2/N_2, and N_2/CH_4 mixtures across SAPO-34 membrane with the Maxwell–Stefan equations, Ind. Eng. Chem. Res. 46 (2007) 3904–3911.
[25] S. Li, J.L. Falconer, R.D. Noble, R. Krishna, Interpreting unary, binary and ternary mixture permeation across a SAPO-34 membrane with loading-dependent Maxwell–Stefan diffusivities, J. Phys. Chem. C 111 (2007) 5075–5082.
[26] R. Krishna, S. Li, J.M. van Baten, J.L. Falconer, R.D. Noble, Investigation of slowing-down and speeding-up effects in binary mixture permeation across SAPO-34 and MFI membranes, Sep. Purif. Technol. 60 (2008) 230–236.
[27] R. Krishna, J.M. van Baten, Segregation effects in adsorption of CO_2 containing mixtures and their consequences for separation selectivities in cage-type zeolites, Sep. Purif. Technol. 61 (2008) 414–423.
[28] J. van den Bergh, W. Zhu, J. Gascon, J.A. Moulijn, F. Kapteijn, Separation and permeation characteristics of a DD3R zeolite membrane, J. Membr. Sci 316 (2008) 35–45.
[29] J. van den Bergh, W. Zhu, J.C. Groen, F. Kapteijn, J.A. Moulijn, K. Yajima, K. Nakayama, T. Tomita, S. Yoshida, Natural gas purification with a DDR zeolite membrane; permeation modelling with Maxwell–Stefan equations, Stud. Surf. Sci. Catal. 170 (2007) 1021–1027.
[30] C. Chmelik, J.M. van Baten, R. Krishna, Hindering effects in diffusion of CO_2/CH_4 mixtures in ZIF-8 crystals, J. Membr. Sci. 397–398 (2012) 87–91.
[31] D. Peralta, G. Chaplais, A. Simon-Masseron, K. Barthelet, G.D. Pirngruber, Separation of C6 paraffins using zeolitic imidazolate frameworks: comparison with zeolite 5A, Ind. Eng. Chem. Res. 51 (2012) 4692–4702.
[32] D. Dubbeldam, R. Krishna, S. Calero, A.Ö. Yazaydın, Computer-assisted screening of ordered crystalline nanoporous adsorbents for separation of alkane isomers, Angew. Chem. Int. Ed. 51 (2012) 11867–11871.
[33] R. Krishna, J.M. van Baten, Comment on modeling adsorption and self-diffusion of methane in LTA zeolites: the influence of framework flexibility, J. Phys. Chem. C 114 (2010) 18017–18021.
[34] R. Krishna, J.M. van Baten, A molecular dynamics investigation of the diffusion characteristics of cavity-type zeolites with 8-ring windows, Micropor. Mesopor. Mater 137 (2011) 83–91.
[35] H. Bux, C. Chmelik, J.M. Van Baten, R. Krishna, J. Caro, Novel MOF-membrane for molecular sieving predicted by IR-diffusion studies and molecular modeling, Adv. Mater. 22 (2010) 4741–4743.
[36] K. Li, D.H. Olson, J. Seidel, T.J. Emge, H. Gong, H. Zeng, J. Li, Zeolitic imidazolate frameworks for kinetic separation of propane and propene, J. Am. Chem. Soc. 131 (2009) 10368–10369.
[37] Y. Pan, T. Li, G. Lestari, Z. Lai, Effective separation of propylene/propane binary mixtures by ZIF-8 membranes, J. Membr. Sci. 390-391 (2012) 93–98.
[38] Y. He, R. Krishna, B. Chen, Metal-organic frameworks with potential for energy-efficient adsorptive separation of light hydrocarbons, Energy Environ. Sci. 5 (2012) 9107–9120.
[39] H. Bux, C. Chmelik, R. Krishna, J. Caro, Ethene/ethane separation by the MOF membrane ZIF-8: molecular correlation of permeation, adsorption, diffusion, J. Membr. Sci. 369 (2011) 284–289.
[40] D.M. Ruthven, S.C. Reyes, Adsorptive separation of light olefins from paraffins, Micropor. Mesopor. Mater. 104 (2007) 59–66.
[41] L. Sandström, E. Sjöberg, J. Hedlund, Very high flux MFI membrane for CO_2 separation, J. Membr. Sci. 380 (2011) 232–240.
[42] O.C. David, D. Gorri, A. Urtiaga, I. Ortiz, Mixed gas separation study for the hydrogen recovery from $H_2/CO/N_2/CO_2$ post combustion mixtures using a Matrimid membrane, J. Membr. Sci. 378 (2011) 359–368.
[43] Z.A.E.P. Vroon, K. Keizer, M.J. Gilde, H. Verweij, A.J. Burggraaf, Transport properties of alkanes through ceramic thin zeolife MFI membranes, J. Membr. Sci. 113 (1996) 293–300.
[44] W.J.W. Bakker, Structured systems in gas separation, Ph.D. Thesis, Delft University of Technology, Delft, 1999.
[45] R. Krishna, J.M. van Baten, Diffusion of hydrocarbon mixtures in MFI zeolite: influence of intersection blocking, Chem. Eng. J. 140 (2008) 614–620.
[46] C.J. Gump, R.D. Noble, J.L. Falconer, Separation of hexane isomers through nonzeolite pores in ZSM-5 zeolite membranes, Ind. Eng. Chem. Res. 38 (1999) 2775–2781.
[47] D.J. Lee, Q. Li, H. Kim, K. Lee, Preparation of Ni-MOF-74 membrane for CO_2 separation by layer-by-layer seeding technique, Micropor. Mesopor. Mater. 163 (2012) 169–177.
[48] E.D. Bloch, W.L. Queen, R. Krishna, J.M. Zadrozny, C.M. Brown, J.R. Long, Hydrocarbon separations in a metal-organic framework with open iron(II) coordination sites, Science 335 (2012) 1606–1610.
[49] P. Peng, B. Shi, Y. Lan, A review of membrane materials for ethanol recovery by pervaporation, Sep. Sci. Technol. 46 (2011) 234–246.
[50] K. Sato, K. Aoki, K. Sugimoto, K. Izumi, S. Inoue, J. Saito, S. Ikeda, T. Nakane, Dehydrating performance of commercial LTA zeolite membranes and application to fuel grade bio-ethanol production by hybrid distillation/vapor permeation process, Micropor. Mesopor. Mater. 115 (2008) 184–188.
[51] K. Sato, K. Sugimoto, N. Shimosuma, T. Kikuchi, T. Kyotani, T. Kurata, Development of practically available up-scaled high-silica CHA-type zeolite membranes for industrial purpose in dehydration of *N*-methyl pyrrolidone solution, J. Membr. Sci. 409-410 (2012) 82–95.
[52] J.Y. Wu, Q.L. Liu, Y. Xiong, A.M. Zhu, Y. Chen, Molecular Simulation of water/alcohol mixtures' adsorption and diffusion in zeolite 4A membranes, J. Phys. Chem. B 113 (2009) 4267–4274.
[53] P. Demontis, J. Gulin-González, H. Jobic, M. Masia, R. Sale, G.B. Suffritti, Dynamical properties of confined water nanoclusters: simulation study of hydrated zeolite NaA: structural and vibrational properties, ACS Nano 2 (2008) 1603–1614.
[54] M.U. Ari, M.G. Ahunbay, M. Yurtsever, A. Erdem-Senatalar, Molecular dynamics simulation of water diffusion in MFI-type zeolites, J. Phys. Chem. B 113 (2009) 8073–8079.
[55] C. Bussai, S. Fritzsche, R. Haberlandt, S. Hannongbua, Formation of low-density water clusters in the silicalite-1 cage: a molecular dynamics study, J. Phys. Chem. B 107 (2003) 12444–12450.
[56] P. Demontis, G. Stara, G.B. Suffritti, Behavior of water in the hydrophobic zeolite silicalite at different temperatures. a molecular dynamics study, J. Phys. Chem. B 107 (2003) 4426–4436.
[57] M. Fleys, R.W. Thompson, Monte Carlo simulations of water adsorption isotherms in silicalite and dealuminated zeolite Y, J. Chem. Theory Comput. 1 (2005) 453–458.
[58] M. Fleys, R.W. Thompson, J.C. MacDonald, Comparison of the behavior of water in silicalite and dealuminated zeolite Y at different temperatures by molecular dynamic simulations, J. Phys. Chem. B 108 (2004) 12197–12203.
[59] L. Narasimhan, P. Boulet, B. Kuchta, O. Schaef, R. Denoyel, P. Brunet, Molecular simulations of water and paracresol in MFI Zeolite – A Monte Carlo study, Langmuir 25 (2009) 11598–11607.
[60] J. Puibasset, R.J.M. Pellenq, Grand Canonical Monte Carlo simulation study of water adsorption in silicalite at 300 K, J. Phys. Chem. B 112 (2008) 6390–6397.
[61] A.Ö. Yazaydın, R.W. Thompson, Molecular simulation of water adsorption in silicalite: effect of silanol groups and different cations, Micropor. Mesopor. Mater. 123 (2009) 169–176.
[62] L. Lu, Q. Shao, L. Huang, X. Lu, Simulation of adsorption and separation of ethanol–water mixture with zeolite and carbon nanotube, Fluid Phase Equilib. 261 (2007) 191–198.
[63] J.Z. Yang, Y. Chen, A.M. Zhu, Q.L. Liu, J.Y. Wu, Analyzing diffusion behaviors of methanol/water through MFI membranes by molecular simulation, J. Membr. Sci. 318 (2008) 327–333.
[64] J.Z. Yang, Q.L. Liu, H.T. Wang, Analyzing adsorption and diffusion behaviors of ethanol/water through silicalite membranes by molecular simulation, J. Membr. Sci. 291 (2007) 1–7.
[65] C. Chmelik, H. Bux, J. Caro, L. Heinke, F. Hibbe, T. Titze, J. Kärger, Mass transfer in a nanoscale material enhanced by an opposing flux, Phys. Rev. Lett. 104 (2010) 085902.

[66] P.Y. Chen, C.P. Chiu, C.W. Hong, Molecular analysis on methanol diffusion in a model nafion membrane, J. Electrochem. Soc. 155 (2008) B1255–B1263.
[67] H. Nasiri, A. Aroujalian, A novel model based on cluster formation for pervaporation separation of polar components from aqueous solutions, Sep. Purif. Technol. 72 (2010) 13–21.
[68] P. Demontis, H. Jobic, M.A. Gonzalez, G.B. Suffritti, Diffusion of water in zeolites NaX and NaY studied by quasi-elastic neutron scattering and computer simulation, J. Phys. Chem. C 113 (2009) 12373–12379.
[69] A. Di Lella, N. Desbiens, A. Boutin, I. Demachy, P. Ungerer, J.P. Bellat, A.H. Fuchs, Molecular simulation studies of water physisorption in zeolites, Phys. Chem. Chem. Phys. 8 (2006) 5396–5406.
[70] I. Halasz, S. Kim, B. Marcus, Uncommon adsorption isotherm of methanol on a hydrophobic Y-zeolite, J. Phys. Chem. B 105 (2001) 10788–10796.
[71] T. Nanok, S. Vasenkov, F. Keil, S. Fritzsche, Molecular dynamics simulation study of the concentration dependence of the self-diffusivity of methanol in NaX zeolite, Micropor. Mesopor. Mater. 127 (2010) 176–181.
[72] D.F. Plant, G. Maurin, R.G. Bell, Modeling the concentration dependence of the methanol self-diffusivity in Faujasite systems: comparison with the liquid phase, J. Phys. Chem. B 110 (2006) 15926–15931.
[73] P. Srinivasa Rao, S. Sridhar, M.Y. Wey, A. Krishnaiah, Pervaporative separation of ethylene glycol/water mixtures by using cross-linked chitosan membranes, Ind. Eng. Chem. Res. 46 (2007) 2155–2163.
[74] J. Caro, M. Bülow, J. Richter-Mendau, J. Kärger, M. Hunger, D. Freude, Nuclear magnetic resonance self-diffusion studies of methanol-water mixtures in pentasil-type zeolites, J. Chem. Soc., Faraday Trans. 83 (1987) 1843–1849.
[75] J.T. Su, P. Brent Duncan, A. Momaya, A. Jutila, D. Needham, The effect of hydrogen bonding on the diffusion of water in *n*-alkanes and *n*-alcohols measured with a novel single microdroplet method, J. Chem. Phys. 132 (2010) 044506.
[76] N. Valentínyi, E. Cséfalvay, P. Mizsey, Modelling of pervaporation: parameter estimation and model development, Chem. Eng. Res. Des. XX (2012) 〈http://www.doi.org/10.1016/j.cherd.2012.07.001〉.
[77] F. Hallberg, T. Vernersson, E.T. Pettersson, S.V. Dvinskikh, G. Lindbergh, I. Furó, Electrokinetic transport of water and methanol in Nafion membranes as observed by NMR spectroscopy, Electrochim. Acta 55 (2010) 3542–3549.
[78] S. Khajavi, J.C. Jansen, F. Kapteijn, Application of hydroxy sodalite films as novel water selective membranes, J. Membr. Sci. 326 (2009) 153–160.
[79] Y. Hasegawa, C. Abe, M. Nishioka, K. Sato, T. Nagase, T. Hanaoka, Formation of high flux CHA-type zeolite membranes and their application to the dehydration of alcohol solutions, J. Membr. Sci. 364 (2010) 318–324.
[80] J. Kuhn, J.M. Castillo-Sanchez, J. Gascon, S. Calero, D. Dubbeldam, T.J.H. Vlugt, F. Kapteijn, J. Gross, Adsorption and diffusion of water, methanol, and ethanol in all-silica DD3R: experiments and simulation, J. Phys. Chem. C 113 (2009) 14290–14301.
[81] Y. Jia, X. Guo, Monte Carlo Simulation of methanol diffusion in critical media, Chinese J. Chem. Eng. 14 (2006) 413–418.
[82] M. Yu, J.L. Falconer, R.D. Noble, R. Krishna, Modeling transient permeation of polar organic mixtures through a MFI zeolite membrane using the Maxwell–Stefan equations, J. Membr. Sci. 293 (2007) 167–173.
[83] B. Bettens, A. Verhoef, H.M. van Veen, C. Vandecasteele, J. Degrève, B. van der Bruggen, Pervaporation of binary water-alcohol and methanol-alcohol mixtures through microporous methylated silica membranes: Maxwell–Stefan modeling, Comput. Chem. Eng. 34 (2010) 1775–1788.
[84] F. de Bruijn, J. Gross, Z. Olujić, P. Jansens, F. Kapteijn, On the driving force of methanol pervaporation through a microporous methylated silica membrane, Ind. Eng. Chem. Res. 46 (2007) 4091–4099.
[85] T. Schultz, K. Sundmacher, Rigorous dynamic model of a direct methanol fuel cell based on Maxwell–Stefan mass transport equations and a Flory–Huggins activity model: formulation and experimental validation, J. Power Sources 145 (2005) 435–462.
[86] T. Schultz, K. Sundmacher, Mass, charge and energy transport phenomena in a polymer electrolyte membrane (PEM) used in a direct methanol fuel cell (DMFC): modelling and experimental validation of fluxes, J. Membr. Sci. 276 (2006) 272–285.
[87] R. Krishna, Adsorptive separation of $CO_2/CH_4/CO$ gas mixtures at high pressures, Micropor. Mesopor. Mater. 156 (2012) 217–223.
[88] R. Krishna, J.M. van Baten, Diffusion of alkane mixtures in zeolites. Validating the Maxwell–Stefan formulation using MD simulations, J. Phys. Chem. B 109 (2005) 6386–6396.
[89] R. Krishna, J.M. van Baten, Diffusion of alkane mixtures in MFI zeolite, Micropor. Mesopor. Mater. 107 (2008) 296–298.
[90] R. Krishna, J.M. van Baten, Investigating the validity of the Knudsen prescription for diffusivities in a mesoporous covalent organic framework, Ind. Eng. Chem. Res. 50 (2011) 7083–7087.
[91] R. Krishna, J.M. van Baten, Investigating the validity of the Bosanquet formula for estimation of diffusivities in mesopores, Chem. Eng. Sci. 69 (2012) 684–688.
[92] R. Krishna, J.M. van Baten, Mutual slowing-down effects in mixture diffusion in zeolites, J. Phys. Chem. C 114 (2010) 13154–13156.
[93] R. Krishna, J.M. van Baten, Hydrogen bonding effects in adsorption of water-alcohol mixtures in zeolites and the consequences for the characteristics of the Maxwell–Stefan diffusivities, Langmuir 26 (2010) 10854–10867.
[94] R. Krishna, J.M. van Baten, Highlighting pitfalls in the Maxwell–Stefan modeling of water–alcohol mixture permeation across pervaporation membranes, J. Membr. Sci. 360 (2010) 476–482.
[95] R. Krishna, J.M. van Baten, Investigating cluster formation in adsorption of CO_2, CH_4, and Ar in zeolites and metal organic frameworks at sub-critical temperatures, Langmuir 26 (2010) 3981–3992.
[96] R. Krishna, J.M. van Baten, Highlighting a variety of unusual characteristics of adsorption and diffusion in microporous materials induced by clustering of guest molecules, Langmuir 26 (2010) 8450–8463.
[97] R. Krishna, J.M. van Baten, A rationalization of the Type IV loading dependence in the Kärger–Pfeifer classification of self-diffusivities, Micropor. Mesopor. Mater. 142 (2011) 745–748.